Subcell monolithic DG/FV–HHO–SSP-RK scheme for a new wave-structure interaction model

Sacha Cardonna[1], David Lannes[2], Fabien Marche[1] & François Vilar[1]

[1] *Institute of Mathematics Alexander Grothendieck, University of Montpellier, France*
[2] *Institute of Mathematics of Bordeaux, University of Bordeaux, France*

SHARK-FV26: Sharing Higher order Advanced Research Known-how on Finite Volume
Minho, Portugal – May 2026

Overview of this talk

Subcell monolithic DG/FV–HHO–SSP-RK scheme for a new **wave-structure interaction** model

---

- **Subcell monolithic DG/FV**: scheme combining DG accuracy with FV robustness for stabilization at the subcell level,
- **Hybrid High-Order**: method designed for elliptic and parabolic PDEs, accurate and low-cost,
- **Strong Stability Preserving Runge Kutta**: high-order time integration scheme for time operators and ODEs,
- **Wave-structure interaction**: model describing rigid objects floating and interacting with waves in shallow water.

Table of contents

Slides available online at sachacardonna.github.io

Table of contents

Slides available online at sachacardonna.github.io

Why are we interested in wave–structure interactions?

Wave–structure interactions arise in many applications where waves interact with floating or partially immersed structures.

- **Offshore engineering**: wave energy converters, floating platforms, coastal protection devices,
- **Nonlinear wave dynamics**: understanding how waves propagate under geometric constraints and transmission conditions,
- **Predictive simulation tools**: deriving models and numerical methods able to describe complex configurations while remaining efficient.

Figure: Wave energy converter (Triton, from Oscilla Power) interacting with ocean waves.

Why is this non-trivial?

Even in simplified shallow-water regimes, wave–structure interactions lead to coupled systems with several mathematical and numerical difficulties.

- **Strong nonlinear coupling**: the fluid and the structure influence each other through pressure, fluxes, and interface conditions,
- **Geometric constraints**: immersed or floating structures introduce constrained regions, moving interfaces, and transmission conditions,
- **Analytical issues**: the well-posedness and stability of the resulting formulations may strongly depend on the chosen coupling strategy,
- **Numerical issues**: robust schemes must preserve the relevant structure of the model while handling nonlinear waves, source terms, and constraints.

*In the following, we will focus on **mathematically well-posed models** rather than purely **engineering-oriented** ones, as we are concerned mainly with the mathematical and numerical challenges of the coupling.*

Table of contents

Slides available online at sachacardonna.github.io

Table of contents

Slides available online at sachacardonna.github.io

3D setting: cylinder structure

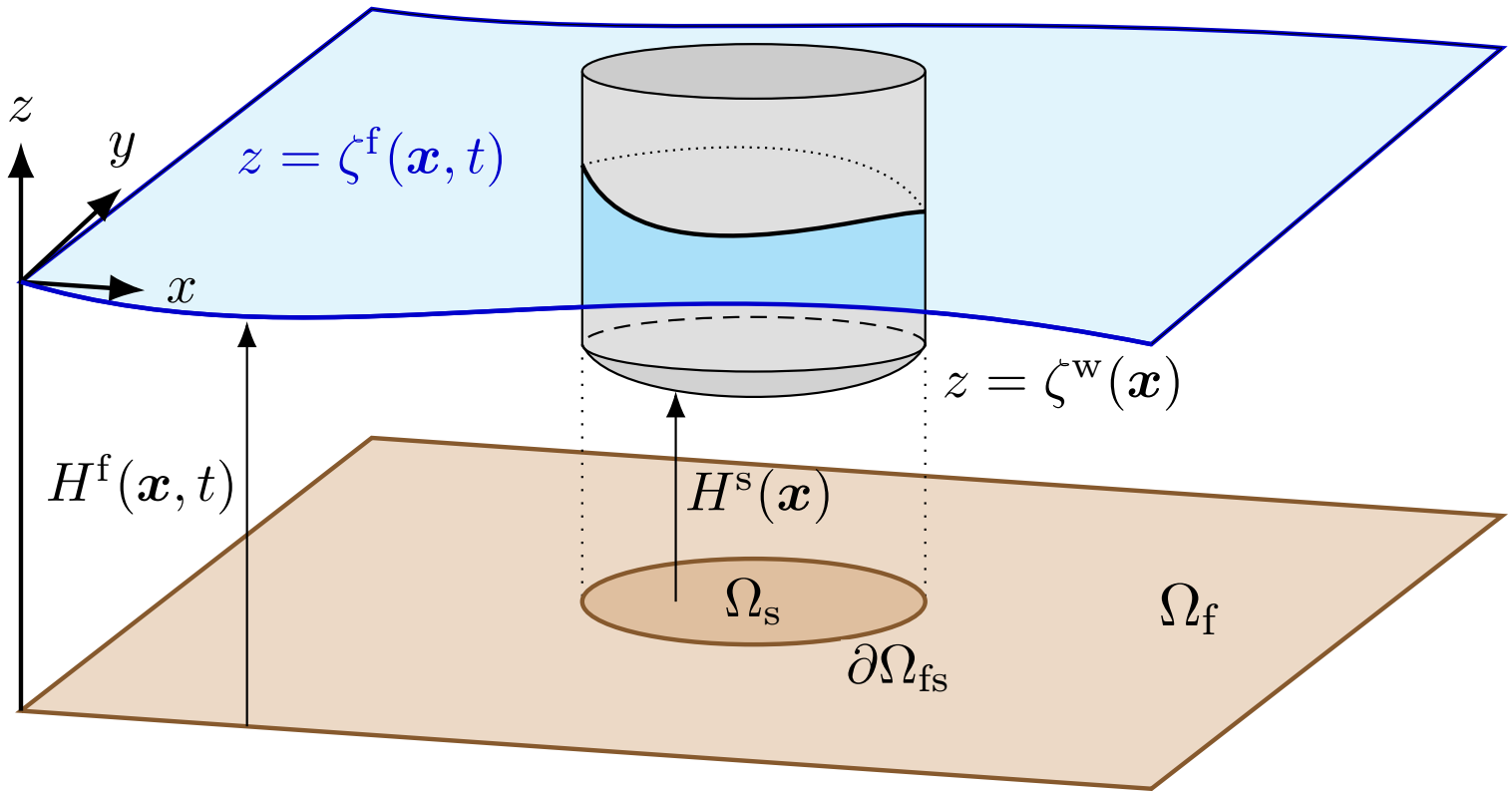

- Fluid domain bounded below by a flat bottom and above by a free surface $z = \zeta(\boldsymbol{x}, t)$,
- A rigid, stationnary, partially immersed floating structure interacts with the surrounding flow,
- Vertical variations are averaged, leading to shallow-water type models.

3D setting: infinite pontoon structure

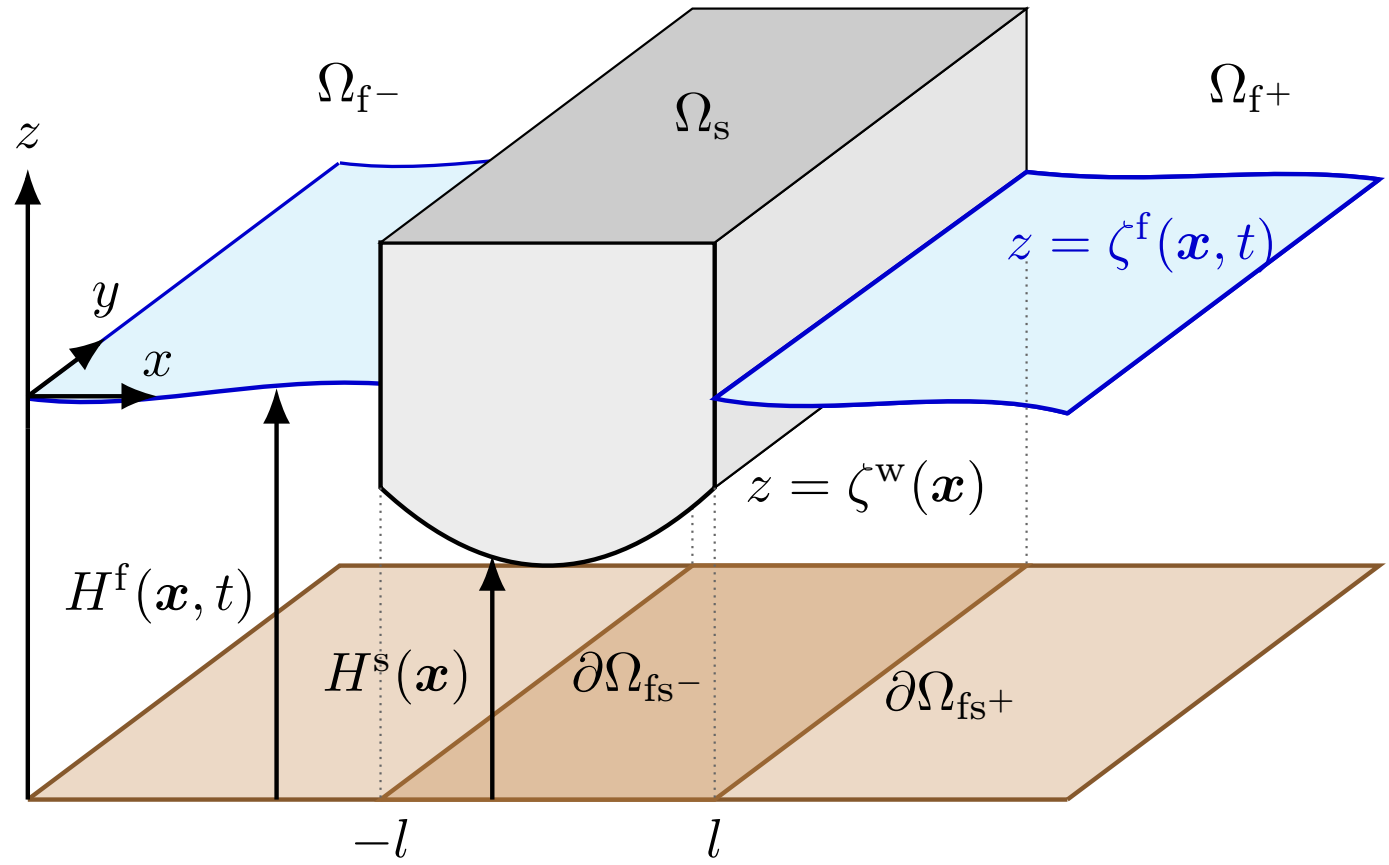

- The interior region is an infinite strip $\Omega_{\mathrm{s}} = (-l, l) \times \mathbb{R}$, while the exterior domain consists of two half-planes $\Omega_{f\pm} = \{(x, y) \mid \pm x > l\}$.
- This configuration provides an **excellent benchmark**, since several quantities can be derived analytically, making it valuable for validation.

2D horizontal setting

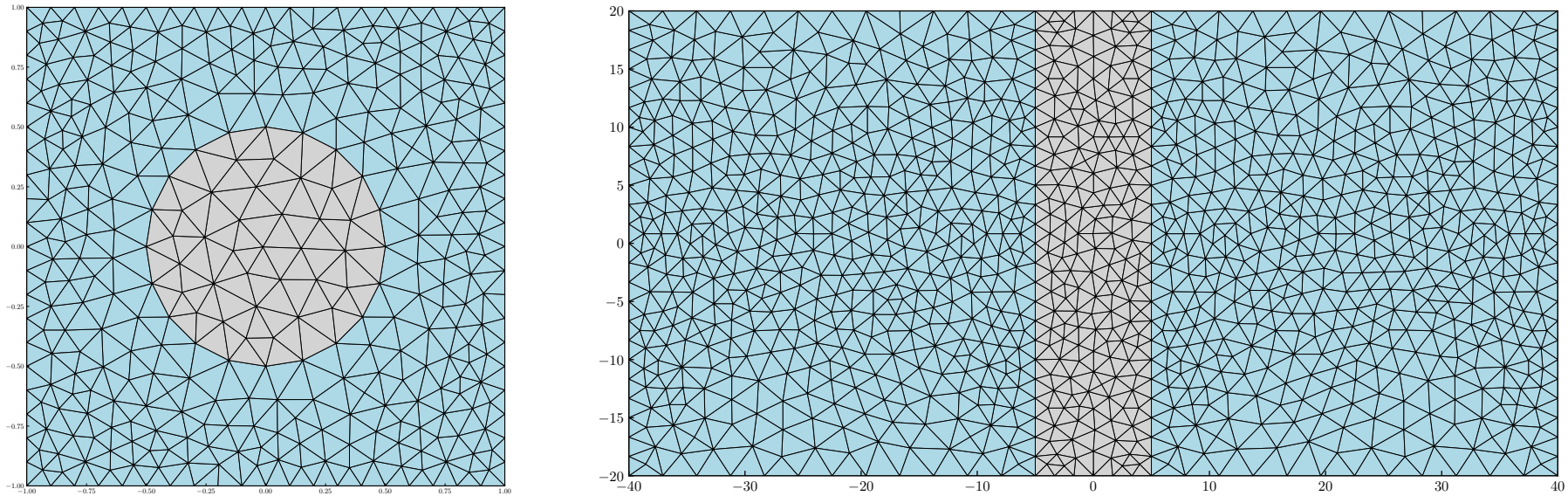

Figure: Computational meshes for a cylinder object (left) and a pontoon-like object (right).

For the latter numerical resolution, we will work in a 2D horizontal setting, where the domain is decomposed into three parts:

- Ω_{s} ("solid region"): hor. projection of the wet part under the object,
- Ω_{f} ("fluid region"): hor. projection of the free surface in contact with air,
- $\partial\Omega_{\mathrm{fs}}$: interface separating them, with unit normal $\mathbf{n}$ pointing toward Ω_{f}.

Notation: we will denote with a superscript $\bullet^{\mathrm{s}}$ (resp. $\bullet^{\mathrm{f}}$) the restriction of a quantity to Ω_{s} (resp. Ω_{f}).

Table of contents

Slides available online at sachacardonna.github.io

Baseline model for water waves

Nonlinear shallow-water (NSW) equations

$$\begin{cases} \partial_t \zeta^{\mathrm{f}} + \nabla_{\boldsymbol{x}} \cdot (H^{\mathrm{f}} \boldsymbol{u}^{\mathrm{f}}) = 0, \\ \partial_t \boldsymbol{u}^{\mathrm{f}} + \boldsymbol{u}^{\mathrm{f}} \cdot \nabla_{\boldsymbol{x}} \boldsymbol{u}^{\mathrm{f}} + \mathrm{g} \nabla_{\boldsymbol{x}} \zeta^{\mathrm{f}} = -\frac{1}{\rho} \nabla_{\boldsymbol{x}} \underline{\mathrm{p}}^{\mathrm{f}}, \end{cases}$$

- $\zeta^{\mathrm{f}} : \mathbb{R}^2 \times (0,T) \mapsto \zeta^{\mathrm{f}}(\boldsymbol{x},t) \in \mathbb{R}$ is the **free surface elevation** with respect to the rest state,
- $\boldsymbol{u}^{\mathrm{f}} : \mathbb{R}^2 \times (0,T) \mapsto \boldsymbol{u}^{\mathrm{f}}(\boldsymbol{x},t) \in \mathbb{R}^2$ is the **depth-averaged horizontal velocity**,
- $H^{\mathrm{f}} : \mathbb{R}^2 \times (0,T) \mapsto H^{\mathrm{f}}(\boldsymbol{x},t) := H_0 + \zeta^{\mathrm{f}}(\boldsymbol{x},t) \in \mathbb{R}_+$ is the **water depth**,
- $\underline{\mathrm{p}}^{\mathrm{f}} : \mathbb{R}^2 \times (0,T) \mapsto \underline{\mathrm{p}}^{\mathrm{f}}(\boldsymbol{x},t) \in \mathbb{R}$ is the **pressure at the free surface**.

Properties of the model

- NSW equations are a **nonlinear** system of **hyperbolic** conservation laws,
- It is valid in the **shallow-water regime** → vertical var. are negligible,
- But it does not account for **dispersive effects** → we chose the "simplest" model to focus on the coupling and numerical issues.

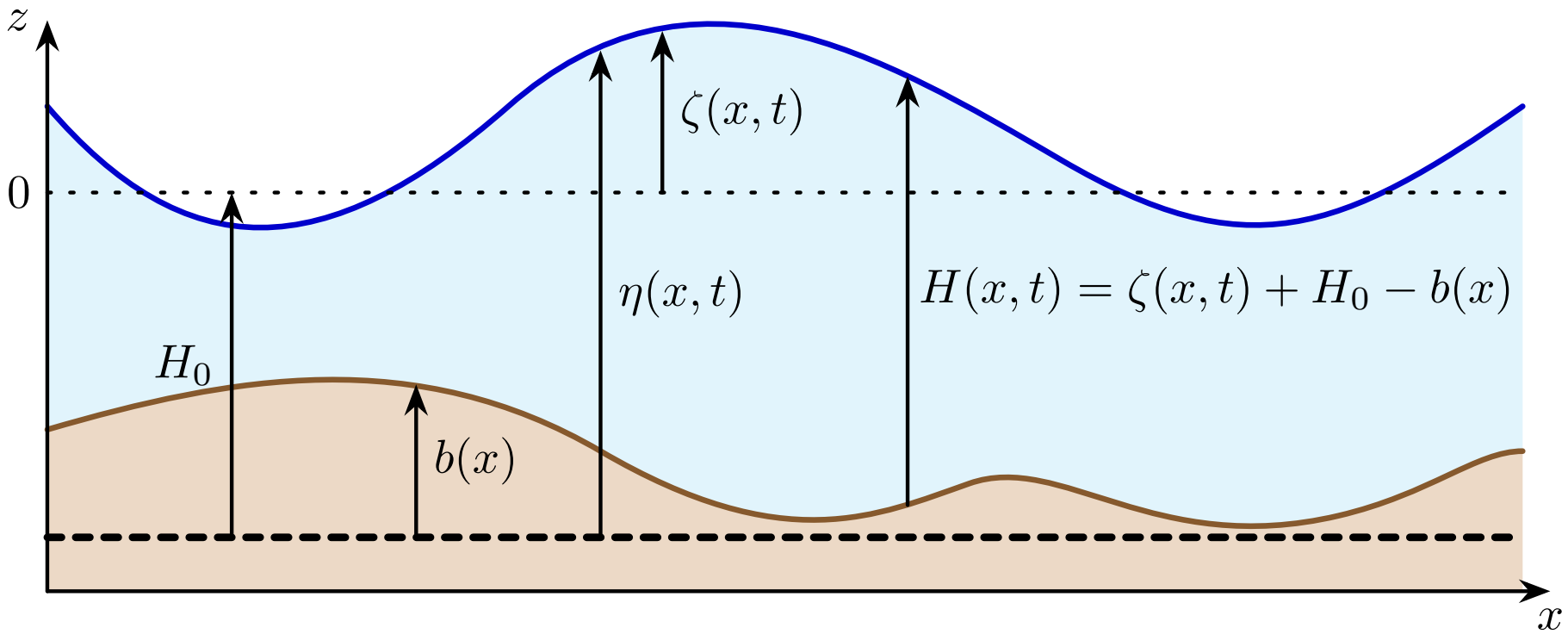

Figure: Shallow-water variables: rest depth H_0, free surface elevation ζ, and total water depth H.

For simplicity, we **neglect topography** as it does not modify the coupling structure nor the transmission conditions, since this source term is purely **geometric** → can be reintroduced later in the numerical experiments!

Table of contents

Slides available online at sachacardonna.github.io

Constraints induced by the floating object

Exterior region Ω_{f} (free surface)

- Surface is in contact with air,
- Pressure prescr.: $\underline{\mathrm{p}} = \mathrm{p}_{\mathrm{atm}}$,
- The NSW momentum equation has no source term:

$$\partial_t \boldsymbol{u}^{\mathrm{f}} + \boldsymbol{u}^{\mathrm{f}} \cdot \nabla_{\boldsymbol{x}} \boldsymbol{u}^{\mathrm{f}} + \mathrm{g} \nabla_{\boldsymbol{x}} \zeta^{\mathrm{f}} = \mathbf{0}.$$

Interior region Ω_{s} (under the object)

- Free surface is blocked by the object (underwater part of the structure),
- Elevation is prescribed: $\zeta^{\mathrm{s}} = \zeta^{\mathrm{w}}$,
- Leads to an "incompressible" constraint: $\nabla_{\boldsymbol{x}} \cdot \boldsymbol{u}^{\mathrm{s}} = 0$.

Coupling at the interface $\partial\Omega_{\mathrm{fs}}$

- Mass conservation (normal flux continuity): $H^{\mathrm{f}} \boldsymbol{u}^{\mathrm{f}} \cdot \mathbf{n} = H^{\mathrm{s}} \boldsymbol{u}^{\mathrm{s}} \cdot \mathbf{n}$,
- Bernouilli pressure transmission (energy consistency): $\Pi^{\mathrm{f}} = \Pi^{\mathrm{s}}$, where $\Pi^{\mathrm{f}} = \rho \mathrm{g} \zeta + \frac{1}{2} \rho |\boldsymbol{u}|^2$ and $\Pi^{\mathrm{s}} = \underline{\mathrm{p}}^{\mathrm{s}} - \mathrm{p}_{\mathrm{atm}} + \rho \mathrm{g} \zeta + \frac{1}{2} \rho |\boldsymbol{u}|^2$,
- Velocity compatibility (no artificial vortex): $\boldsymbol{u}^{\mathrm{f}} \cdot \mathbf{n}^{\perp} = \boldsymbol{u}^{\mathrm{s}} \cdot \mathbf{n}^{\perp}$.

Summary: a coupled "partly constrained" SW system

A first wave–structure interaction model

- Exterior region Ω_{f} (free surface):

$$\partial_t \zeta^{\mathrm{f}} + \nabla_{\boldsymbol{x}} \cdot (H^{\mathrm{f}} \boldsymbol{u}^{\mathrm{f}}) = 0$$
$$\partial_t \boldsymbol{u}^{\mathrm{f}} + \boldsymbol{u}^{\mathrm{f}} \cdot \nabla_{\boldsymbol{x}} \boldsymbol{u}^{\mathrm{f}} + \mathrm{g} \nabla_{\boldsymbol{x}} \zeta^{\mathrm{f}} = \mathbf{0}$$

Nonlinear shallow-water equations

- Interior region Ω_{s} (under the object):

$$\nabla_{\boldsymbol{x}} \cdot \boldsymbol{u}^{\mathrm{s}} = 0$$
$$\partial_t \boldsymbol{u}^{\mathrm{s}} + \boldsymbol{u}^{\mathrm{s}} \cdot \nabla_{\boldsymbol{x}} \boldsymbol{u}^{\mathrm{s}} = \rho^{-1} \nabla_{\boldsymbol{x}} \underline{\mathrm{p}}^{\mathrm{s}}$$

Incompressible Euler equations

- Interface $\partial\Omega_{\mathrm{fs}}$ (coupling conditions):

$$H^{\mathrm{f}} \boldsymbol{u}^{\mathrm{f}} \cdot \mathbf{n} = H^{\mathrm{s}} \boldsymbol{u}^{\mathrm{s}} \cdot \mathbf{n} \qquad \textit{Mass flux continuity}$$
$$\Pi^{\mathrm{f}} = \Pi^{\mathrm{s}} \qquad \textit{Bernoulli pressure continuity}$$
$$\boldsymbol{u}^{\mathrm{f}} \cdot \mathbf{n}^{\perp} = \boldsymbol{u}^{\mathrm{s}} \cdot \mathbf{n}^{\perp} \qquad \textit{Tangential continuity}$$

Irrotational initial data: a key simplification

Propagation of irrotationality

If $\nabla_{\boldsymbol{x}}^{\perp} \cdot \boldsymbol{u}^{\mathrm{f}}(\cdot, 0) = 0$ in Ω_{f} and $\nabla_{\boldsymbol{x}}^{\perp} \cdot \boldsymbol{u}^{\mathrm{s}}(\cdot, 0) = 0$ in Ω_{s}, it stays true for all $t \geq 0$

$\hookrightarrow$ Physically the flow remains smooth, without rotation or vortex generation.

Consequence: the interior becomes elliptic

- Because the flow remains **irrotational**, the interior velocity can be written as a **gradient field** $i.e.$ there exists a potential ϕ^{s} such that

$$\boldsymbol{u}^{\mathrm{s}} = \nabla_{\boldsymbol{x}} \phi^{\mathrm{s}} \quad \text{in } \Omega_{\mathrm{s}}.$$

- Under the object, the free surface is fixed, hence the water depth is **constant in time**: $\partial_t H^{\mathrm{s}} = \partial_t (H_0 + \zeta^{\mathrm{w}}) = 0$.
- Combining irrotationality with the incompressibility constraint $\nabla_{\boldsymbol{x}} \cdot \boldsymbol{u}^{\mathrm{s}} = 0$ leads to an **elliptic problem** for the potential:

$$\boxed{\nabla_{\boldsymbol{x}} \cdot \left(H^{\mathrm{s}} \nabla_{\boldsymbol{x}} \phi^{\mathrm{s}} \right) = 0 \quad \text{in } \Omega_{\mathrm{s}}}$$

From the interior constraint to a mixed formulation

What happens under the object

- To solve $\nabla_{\boldsymbol{x}} \cdot \left(H^{\mathrm{s}} \nabla_{\boldsymbol{x}} \phi^{\mathrm{s}} \right) = 0$ in Ω_{s}, we prescribe the trace of the potential on the interface,
$$\phi^{\mathrm{s}} = \psi^{\mathrm{s}} \quad \text{on } \partial\Omega_{\mathrm{fs}}.$$
- The trace ψ^{s} is **not arbitrary**: it evolves in time according to an ODE obtained from the Bernoulli relation on the interface,
$$\partial_t \psi^{\mathrm{s}} = -\mathrm{g}\zeta - \frac{1}{2}|\boldsymbol{u}|^2 \quad \text{on } \partial\Omega_{\mathrm{fs}}.$$

How the interior talks to the exterior

We define the following **Dirichlet–Neumann operator:**

$$\boxed{\Lambda\psi^{\mathrm{s}} := H^{\mathrm{s}} \nabla_{\boldsymbol{x}} \phi^{\mathrm{s}} \cdot \mathbf{n} \quad \text{on } \partial\Omega_{\mathrm{fs}}}$$

maps the potential ψ^{s} (Dirichlet data) to the normal flux (Neumann data)

↪ Quantifies how the interior motion exchanges water with the exterior flow

Digression: the infinite pontoon case (1)

Infinite pontoon and generalized Dirichlet–Neumann operator

We prescribe the traces of the interior potential, i.e. $\phi^{\mathrm{s}} = \psi_{\pm}$ on $\partial\Omega_{\mathrm{fs}^{\pm}} := \{(\pm l, y) \mid y \in \mathbb{R}\}$ and for $\boldsymbol{\psi}^{\mathrm{s}} = (\psi_-, \psi_+)$ define

$$\boldsymbol{\Lambda}\boldsymbol{\psi}^{\mathrm{s}} = \big(\Lambda_-\boldsymbol{\psi}^{\mathrm{s}}, \Lambda_+\boldsymbol{\psi}^{\mathrm{s}}\big), \qquad \Lambda_\pm\boldsymbol{\psi}^{\mathrm{s}} = \pm H^{\mathrm{s}}(\partial_x\phi^{\mathrm{s}})_{|x=\pm l}.$$

Why this configuration matters?

Because the **Dirichlet-Neumann operator** can then be written **explicitly** as:

$$\Lambda_-\boldsymbol{\psi}^{\mathrm{s}}(y) = H^{\mathrm{s}}\,\mathfrak{F}^{-1}\Big(\xi\coth(2\ell\xi)\,\widehat{\psi}_-(\xi)\Big)(y) - H^{\mathrm{s}}\,\mathfrak{F}^{-1}\Big(\tfrac{\xi}{\sinh(2\ell\xi)}\,\widehat{\psi}_+(\xi)\Big)(y),$$

$$\Lambda_+\boldsymbol{\psi}^{\mathrm{s}}(y) = -H^{\mathrm{s}}\,\mathfrak{F}^{-1}\Big(\tfrac{\xi}{\sinh(2\ell\xi)}\,\widehat{\psi}_-(\xi)\Big)(y) + H^{\mathrm{s}}\,\mathfrak{F}^{-1}\Big(\xi\coth(2\ell\xi)\,\widehat{\psi}_+(\xi)\Big)(y),$$

where $\widehat{\psi}_\pm = \mathfrak{F}(\psi_\pm)$ denotes the Fourier transform with respect to the transverse variable y.

↪ No **elliptic solver** is needed inside the structure, which makes an ideal benchmark to validate the coupling strategy **independently** of the interior solver!

Digression: the infinite pontoon case (2)

Discrete Fourier transform for efficient evaluation

When the solution **genuinely depends** on y, the explicit operator can be evaluated efficiently by **Fast Fourier Transform (FFT)**, keeping the pontoon case computationally inexpensive.

Transverse-invariant case: reduction to a 1D model

Assume that the solution **does not** depend on y, then the fully two-dimensional pontoon model reduces to a classical **one-dimensional wave–structure interaction system**, where the interior motion is described by a single discharge variable

$$q^{\mathrm{s}}(t) = \frac{H^{\mathrm{s}}}{2l}\big(\psi_+ - \psi_-\big),$$

which satisfies

$$\frac{\mathrm{d}q^{\mathrm{s}}}{\mathrm{d}t}(t) = -\frac{H^{\mathrm{s}}}{2l}\big(\Pi_+ - \Pi_-\big).$$

↪ The structure behaves symply as a **dynamic transmission law** between the left and right waves!

Equivalent mixed formulation (irrotational case)

Exterior hyperbolic problem with boundary coupling

- Exterior region Ω_{f} (free surface):

$$\partial_t \zeta^{\mathrm{f}} + \nabla_{\boldsymbol{x}} \cdot (H^{\mathrm{f}} \boldsymbol{u}^{\mathrm{f}}) = 0$$
$$\partial_t \boldsymbol{u}^{\mathrm{f}} + \boldsymbol{u}^{\mathrm{f}} \cdot \nabla_{\boldsymbol{x}} \boldsymbol{u}^{\mathrm{f}} + \mathrm{g} \nabla_{\boldsymbol{x}} \zeta^{\mathrm{f}} = \boldsymbol{0}$$

Nonlinear shallow-water equations

- Interior region Ω_{s} (object):

$$\nabla_{\boldsymbol{x}} \cdot \left(H^{\mathrm{s}} \nabla_{\boldsymbol{x}} \phi^{\mathrm{s}} \right) = 0 \quad \text{in } \Omega_{\mathrm{s}}$$
$$\phi^{\mathrm{s}} = \psi^{\mathrm{s}} \quad \text{on } \partial\Omega_{\mathrm{fs}}$$

Elliptic equation on potential

- Interface $\partial\Omega_{\mathrm{fs}}$ (boundary coupling):

$$\mathbf{n} \cdot (H \boldsymbol{u}) = \Lambda \psi^{\mathrm{s}}$$

Normal flux from the interior

$$\partial_t \psi^{\mathrm{s}} = -\mathrm{g}\zeta - \tfrac{1}{2} |\boldsymbol{u}|^2$$

Bernoulli ODE

- Initial conditions: $(\zeta^{\mathrm{f}}, \boldsymbol{u}^{\mathrm{f}})_{|t=0} = (\zeta^{\mathrm{in}}, \boldsymbol{u}^{\mathrm{in}})$ in Ω_{f} and $\psi^{\mathrm{s}}_{|t=0} = \psi^{\mathrm{s}}_{\mathrm{in}}$ on $\partial\Omega_{\mathrm{fs}}$.

Table of contents

Slides available online at sachacardonna.github.io

Numerical challenges induced by the coupled model

What makes wave–structure simulations difficult?

- **Two types of PDEs:** **hyperbolic** NSW in Ω_{f}, **elliptic** PDE to compute DN operator on $\partial\Omega_{\mathrm{fs}}$ with a strong coupling,
- **Nonlinearities and discontinuities:** hyperbolicity and nonlinearity imply solutions can become **discontinuous** in finite time,
- **Geometry:** dealing with **unstructured meshes** and **complex geometries** is more challenging than simple Cartesian meshes.

What we want from the discretization

- **High-order accuracy** to capture every singularities and nonlinear effects,
- **Robustness** near shocks and wet/dry fronts (if topography is included),
- **Preservation of physical properties** (e.g. positivity of water depth, energy consistency)...

$\hookrightarrow$ These requirements are often in tension, and designing a scheme that satisfies all of them is non-trivial!

Table of contents

Slides available online at sachacardonna.github.io

Two classical approaches for hyperbolic PDEs

Finite Volume (FV)

- Integral formulation over control volumes $\omega_c \subset \Omega$ with $\Omega = \bigcup \omega_c$;
- Piecewise constant approximation:

$$\boldsymbol{v}_h^c(t) \simeq \frac{1}{|\omega_c|} \int_{\omega_c} \boldsymbol{v}(\boldsymbol{x}, t)\, \mathrm{d}\boldsymbol{x},$$

  where $\boldsymbol{v}$ is the exact solution;
- Numerical flux $\mathbb{F}^*$ ensures conservation and stability.

✔ Robust and easy to implement, well-suited for nonlinear problems,

✖ Low-order accuracy unless polynomial reconstruction is applied.

Discontinuous Galerkin (DG)

- Weak formulation on each element $\omega_c \subset \Omega$ with $\Omega = \bigcup \omega_c$;
- Piecewise polynomial approx.:

$$\boldsymbol{v}_h^c(\boldsymbol{x}, t) = \sum_{m=1}^{\dim \mathbb{P}^k} \boldsymbol{v}_m^c(t)\, \psi_m^c(\boldsymbol{x}),$$

  with test functions in $\mathbb{P}^k(\omega_c)$;
- Numerical flux $\mathbb{F}^*$ to ensure local conservation.

✔ High-order accuracy with compact stencil, well-suited for parallelism,

✖ Less robust, more complex implementation and prone to oscillations.

Stabilization principle

⚠ When you design high-order schemes, you need to add some form of **stabilization** to prevent non-physical oscillations near discontinuities and ensure the robustness of the method.

- **Classical stabilization:** apply limiters/a posteriori correction on the full cell

  ↪ risks **discarding** a mostly accurate solution due to a **local failure**

- **Subcell approach:** partition each cell into finer subcells to reduce the correction scale

  ↪ enabling a **surgical correction**, meaning only fix what's necessary, preserving as much of the high-order DG content as possible

Theory needed – Reformulation of DG as a subcell FV-like scheme

A little state-of-the-art on subcell stabilization

- **Classical *a posteriori* subcell paradigm:** once a cell is flagged as troubled, its high-order DG update is discarded and completely recomputed using a robust finite-volume scheme on the subcells,
- **Recent monolithic/blended paradigms:** perform a single-step update by locally blending high-order DG and low-order FV fluxes; stabilization is applied directly at the subcell interfaces avoiding full cell recomputation.

Some pioneering references for this presentation

M. Sonntag & C. D. Munz, *Shock capturing for discontinuous Galerkin methods using finite volume subcells*. Finite Volumes for Complex Applications VII, pp. 945–953. Springer, 2014.

M. Dumbser & R. Loubère, *A simple robust and accurate a posteriori subcell finite volume limiter for the discontinuous Galerkin method on unstructured meshes*. J. Comp. Phys., 2016.

A. Rueda-Ramírez, B. Bolm, D. Kuzmin & G. Gassner, *Monolithic convex limiting for Legendre-Gauss-Lobatto Discontinuous Galerkin Spectral-Element methods*. Commun. Appl. Math., 2024.

A classical mesh ...

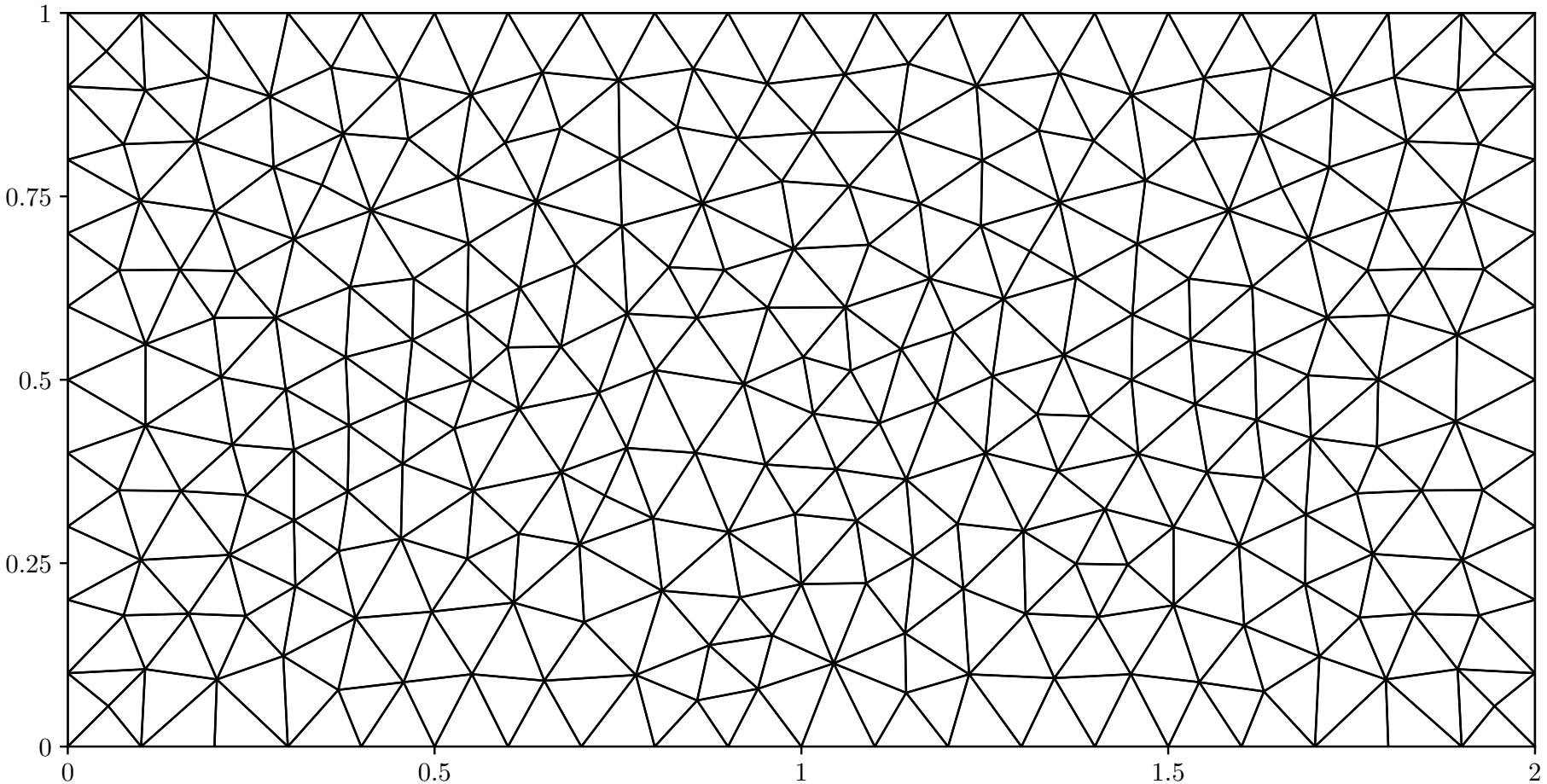

Figure: Unstructured simplicial mesh with $n_{\text{el}} = 350$ cells.

... and its subdivision

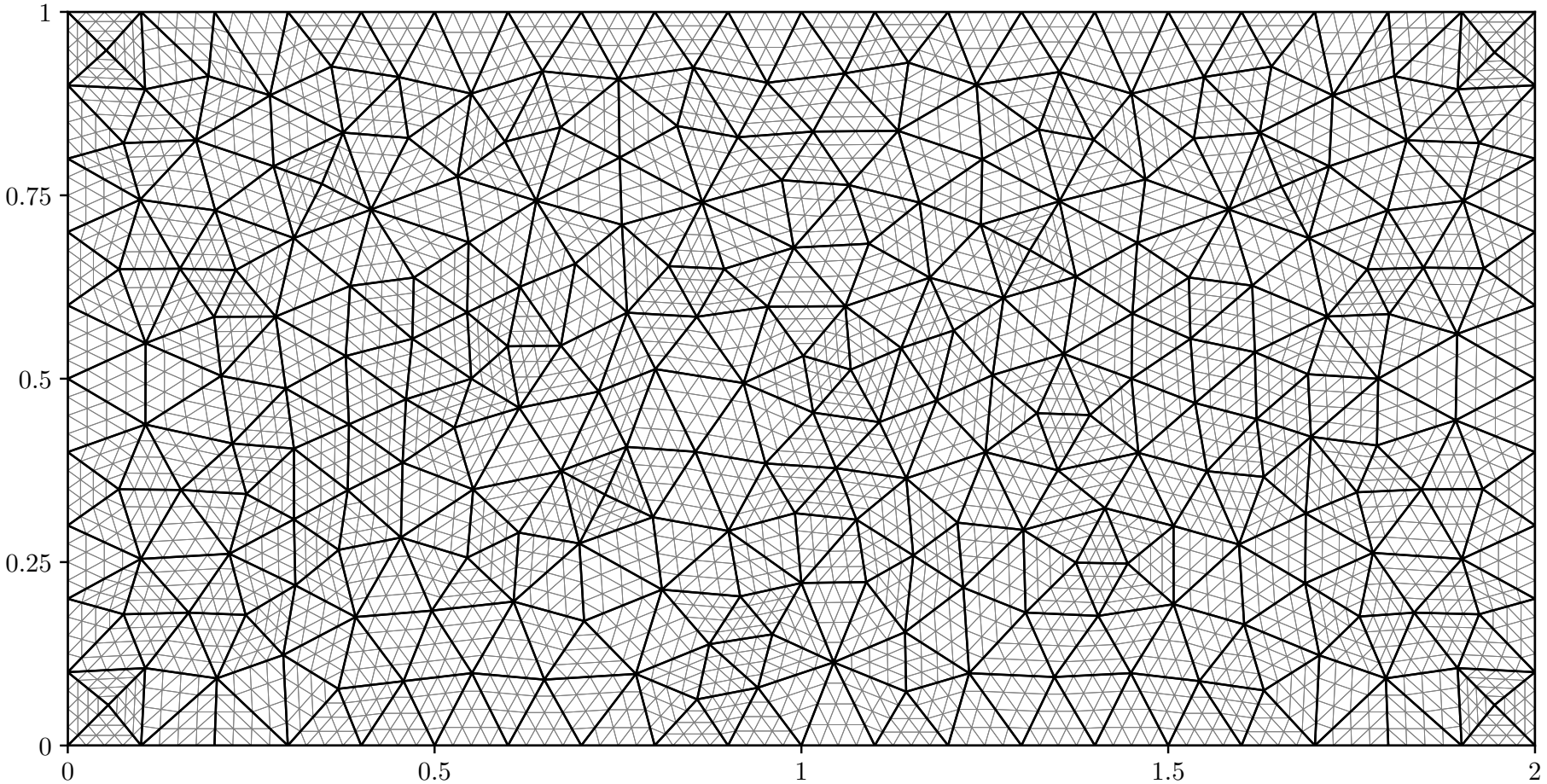

Figure: Unstructured simplicial mesh $\mathbb{P}^3$ subdivision onto triangles with $n_{\text{el}} = 350$ cells.

Monolithic DG/FV idea (hyperbolic solver)

Best of both worlds between precision and robustness

- DG is high-order accurate but may oscillate near discontinuities,
- FV is robust (in particular positivity-friendly) but low-order,

Monolithic DG/FV schemes blend the two approaches in a single framework, with a local correction of the DG solution where needed.

Key ingredient: subcell viewpoint

Considering $\boldsymbol{v}_h^c$ the DG numerical solution on each cell $\omega_c \subset \Omega_\mathrm{f}$, we build a sub-partition $\{S_m^c\}_{m=1}^{N_s} := \{S_1^c, S_2^c, \ldots, S_{N_s}^c\}$ and track subcell averages

$$\boxed{\overline{\boldsymbol{v}}_m^c(t) = \frac{1}{|S_m^c|} \int_{S_m^c} \boldsymbol{v}_h^c(\boldsymbol{x}, t)\, \mathrm{d}\boldsymbol{x}}$$

F. Vilar, *Local subcell monolithic DG/FV convex property preserving scheme on unstructured grids and entropy consideration*. JCP, 2025.

S.C., F. Marche & F. Vilar, *An high-order scheme for 2D NSW equations with topography and friction effects on unstructured grids*. JCP (rev.), 2026.

Submean values and polynomial moments

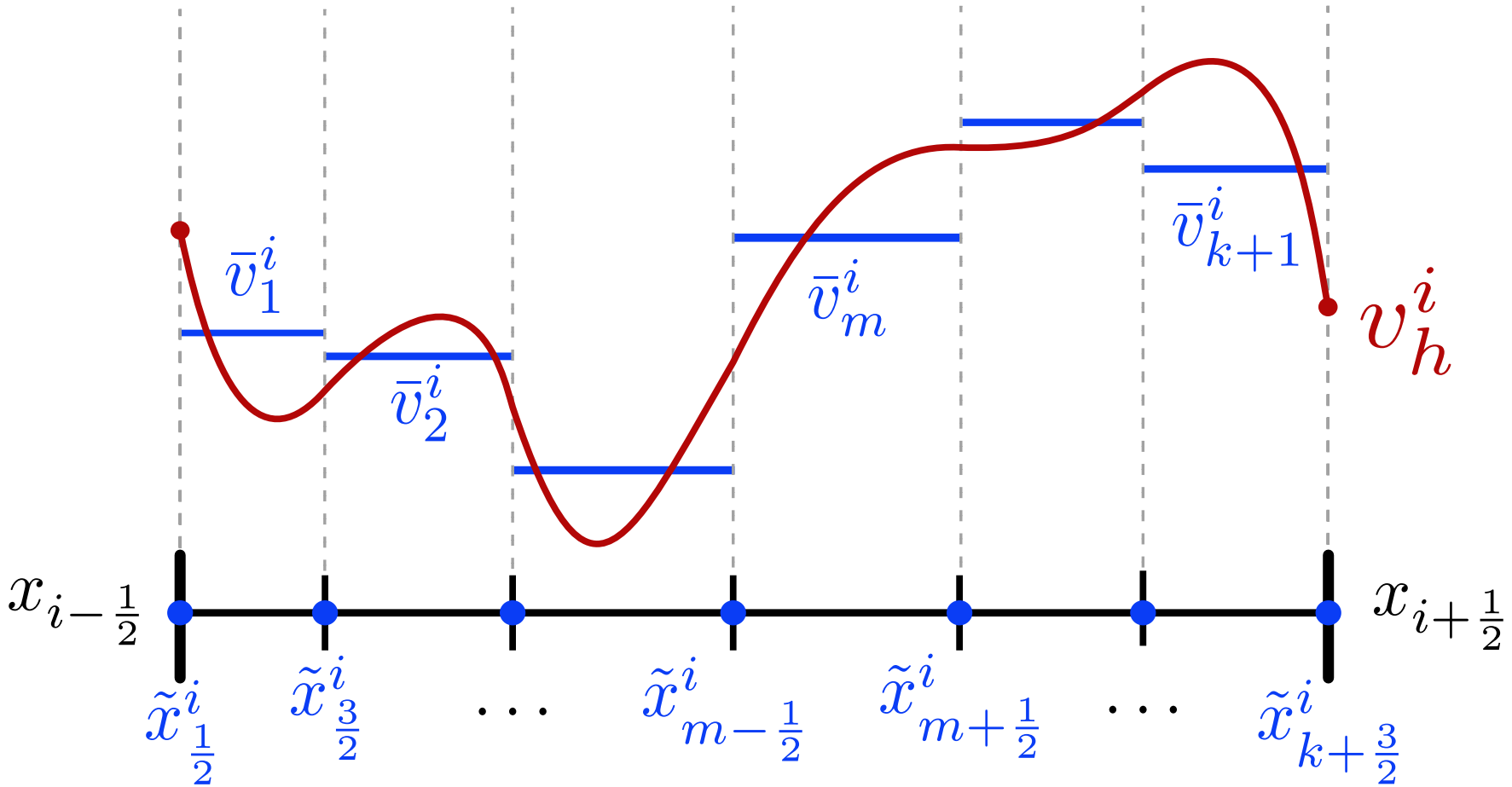

Figure: Piecewise polynomial function v_h^i and associated sub-mean-values (1D case).

Flux blending and fully-discrete scheme

Blended numerical flux

On each subface Γ_{mp}^c of each subcell S_m^c, we combine two fluxes:

- a high-order reconstructed **DG flux** $\widehat{\mathbb{F}}_{mp}$, precise but oscillatory,
- a first-order domain-invariant **FV flux** $\mathbb{F}_{mp}^{*,\mathsf{FV}}$, very robust but less accurate,

$$\boxed{\widetilde{\mathbb{F}}_{mp} = \mathbb{F}_{mp}^{*,\mathsf{FV}} + \Theta_{mp}\left(\widehat{\mathbb{F}}_{mp} - \mathbb{F}_{mp}^{*,\mathsf{FV}}\right)}$$

⚠ The **blending coefficient** $\Theta_{mp} \in [0,1]$ is:

- computed $a\,priori$ on each Γ_{mp}^c, at each time step (or RK stage),
- uniquely defined $i.e.$ $\Theta_{mp} = \Theta_{pm}$, for all $S_p^v \in \mathscr{V}_m^c$.

$\hookrightarrow$ Θ_{mp} controls the balance between **accuracy** and **robustness**!

Local subcell monolithic DG/FV scheme for the hyperbolic part (NSW)

$$\overline{\boldsymbol{v}}_m^{c,n+1} = \overline{\boldsymbol{v}}_m^{c,n} - \frac{\Delta t^n}{|S_m^c|} \sum_{S_p^v \in \mathrm{Neigh}(S_m^c)} |\Gamma_{mp}^c|\, \widetilde{\mathbb{F}}_{mp}, \quad \forall S_m^c \in \{S_j^c\}_{j=1}^{N_s}, \quad \forall \omega_c \subset \Omega_{\mathrm{f}}.$$

Table of contents

Slides available online at sachacardonna.github.io

Hybrid High-Order (HHO) scheme for the interior elliptic problem

Elliptic solver for the Dirichlet–Neumann operator

In the general geometry, the Dirichlet–Neumann operator is not explicit; we therefore compute it by solving the interior problem

$$\nabla_{\boldsymbol{x}} \cdot \left(H^{\mathrm{s}} \nabla_{\boldsymbol{x}} \phi^{\mathrm{s}} \right) = 0 \quad \text{in } \Omega_{\mathrm{s}}, \qquad \phi^{\mathrm{s}} = \psi^{\mathrm{s}} \quad \text{on } \partial\Omega_{\mathrm{fs}}.$$

↪ **Hybrid High-Order** (HHO) method is used to solve this elliptic equation.

Discrete HHO unknowns

Cell and face unknowns (polynomials of degree k):

$$\phi_c^{\mathrm{s}} \in \mathbb{P}^k(\omega_c), \qquad \phi_\Gamma^{\mathrm{s}} \in \mathbb{P}^k(\Gamma), \qquad \omega_c \subset \Omega_{\mathrm{s}},\ \Gamma \subset \partial\omega_c.$$

- **Hybrid viewpoint:** cell unknowns represent the interior behaviour, while face unknowns control how neighbouring cells communicate,
- **Local reconstruction:** a high-order approximation of the gradient is built inside each cell, reproducing the continuous integration-by-parts structure,
- **Computational efficiency:** cell unknowns are eliminated locally, so the global problem involves face unknowns only.

Structure of the discrete HHO problem

Global formulation

We introduce the **global HHO space of degree** k:

$$\mathrm{HHO}^k := \left\{ \underline{\phi}_h^{\mathrm{s}} = \left((\phi_c^{\mathrm{s}})_c, (\phi_\Gamma^{\mathrm{s}})_\Gamma \right) \;\middle|\; \phi_c^{\mathrm{s}} \in \mathbb{P}^k(\omega_c),\ \phi_\Gamma^{\mathrm{s}} \in \mathbb{P}^k(\Gamma) \right\}.$$

The discrete interior problem reads: find $\underline{\phi}_h^{\mathrm{s}} \in \mathrm{HHO}^k_{\mathrm{dir}}$ such that

$$\mathscr{A}_h^{\mathrm{s}}(\underline{\phi}_h^{\mathrm{s}}, \underline{w}_h) = \sum_{\omega_c^{\mathrm{s}} \subset \Omega_{\mathrm{s}}} \mathscr{A}_c^{\mathrm{s}}(\underline{\phi}_c^{\mathrm{s}}, \underline{w}_c) = 0, \qquad \forall \underline{w}_h \in \mathrm{HHO}^k_{\mathrm{hom}}.$$

Algebraic formulation

The bilinear form $\mathscr{A}_h^{\mathrm{s}}$ translates into stiffness blocks $\mathbb{K}_{\alpha\beta}$ (gradient reconstructions + stabilization), while $\boldsymbol{g}$ contains the Dirichlet boundary data ψ^{s}:

$$\begin{bmatrix} \mathbb{K}_{cc} & \mathbb{K}_{c\Gamma} \\ \mathbb{K}_{\Gamma c} & \mathbb{K}_{\Gamma\Gamma} \end{bmatrix} \begin{bmatrix} \underline{\phi}_c \\ \underline{\phi}_\Gamma \end{bmatrix} = \begin{bmatrix} \mathbf{0} \\ \boldsymbol{g} \end{bmatrix}$$

↪ **Static condensation:** since $\mathbb{K}_{cc}$ is **block-diagonal** (cells only interact via faces), cell unknowns $\underline{\phi}_c$ are locally eliminated to solve a global system on faces only:

$$\left(\mathbb{K}_{\Gamma\Gamma} - \mathbb{K}_{\Gamma c} \mathbb{K}_{cc}^{-1} \mathbb{K}_{c\Gamma} \right) \underline{\phi}_\Gamma = \boldsymbol{g}$$

Table of contents

Slides available online at sachacardonna.github.io

A new wave–structure interaction numerical coupling

How equations talk to each other

1. The following ODE is solved reading the values of ζ and $\boldsymbol{u}$ at the interface

$$\partial_t \psi^{\mathrm{s}} = -\mathrm{g}\zeta - \tfrac{1}{2}|\boldsymbol{u}|^2 \quad \text{on } \partial\Omega_{\mathrm{fs}} \qquad \textbf{SSP-RK scheme}$$

2. The trace ψ^{s} is used as a Dirichlet boundary condition to solve the interior elliptic problem

$$\begin{aligned} \nabla_{\boldsymbol{x}} \cdot \left(H^{\mathrm{s}} \nabla_{\boldsymbol{x}} \phi^{\mathrm{s}}\right) &= 0 \quad \text{in } \Omega_{\mathrm{s}} \\ \phi^{\mathrm{s}} &= \psi^{\mathrm{s}} \quad \text{on } \partial\Omega_{\mathrm{fs}} \end{aligned} \qquad \textbf{Hybrid High-Order scheme}$$

3. The normal flux at the interface is computed from the Dirichlet–Neumann operator $\Lambda\psi^{\mathrm{s}} := H^{\mathrm{s}} \nabla_{\boldsymbol{x}} \phi^{\mathrm{s}} \cdot \mathbf{n}$ and used as a boundary condition for the exterior hyperbolic problem in Ω_{f}:

$$\begin{aligned} \partial_t \zeta^{\mathrm{f}} + \nabla_{\boldsymbol{x}} \cdot (H^{\mathrm{f}} \boldsymbol{u}^{\mathrm{f}}) &= 0 \\ \partial_t \boldsymbol{u}^{\mathrm{f}} + \boldsymbol{u}^{\mathrm{f}} \cdot \nabla_{\boldsymbol{x}} \boldsymbol{u}^{\mathrm{f}} + \mathrm{g} \nabla_{\boldsymbol{x}} \zeta^{\mathrm{f}} &= \mathbf{0} \end{aligned} \qquad \textbf{Monolithic DG/FV scheme}$$

↪ The time integration is handled using a **SSP-RK scheme**.

Table of contents

Slides available online at sachacardonna.github.io

Comparison between analytical and numerical DN operators

Wave propagation under a fixed floating structure

- **Domain:** $\Omega = [-40, 40] \times [-20, 20]$ **Degree:** $k = 2$ **Mesh:** $n_{\text{el}} = 892$
- **Goal:** validate the numerical HHO DN operator by comparing it to the analytical Fourier solution for the fixed pontoon (MP4)

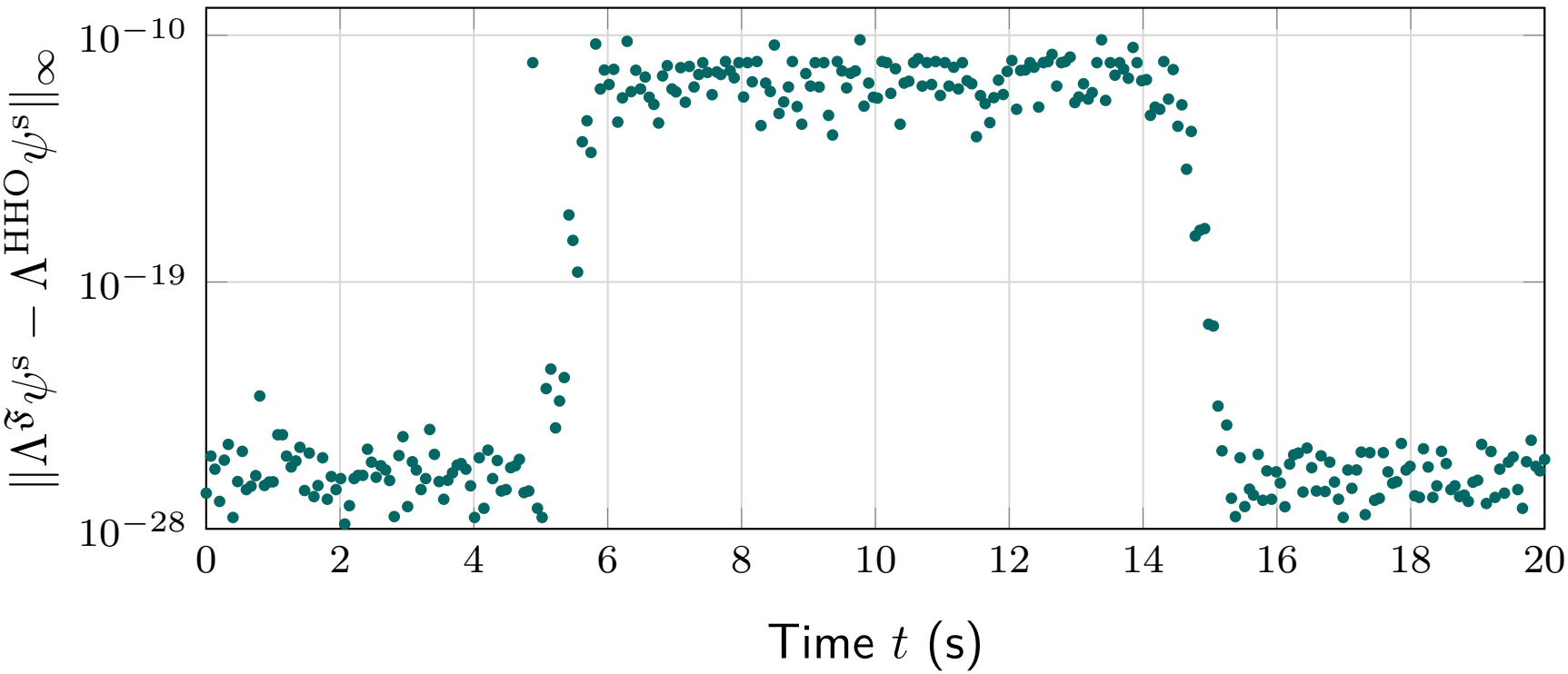

Some qualitative simulations

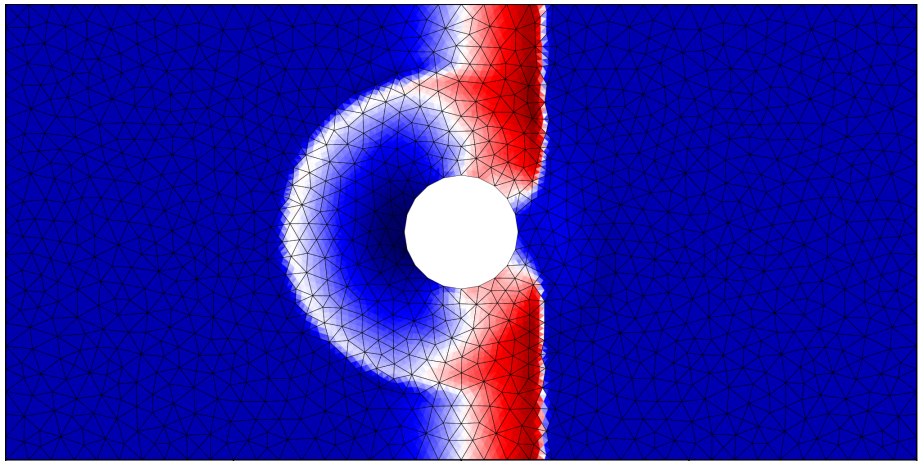
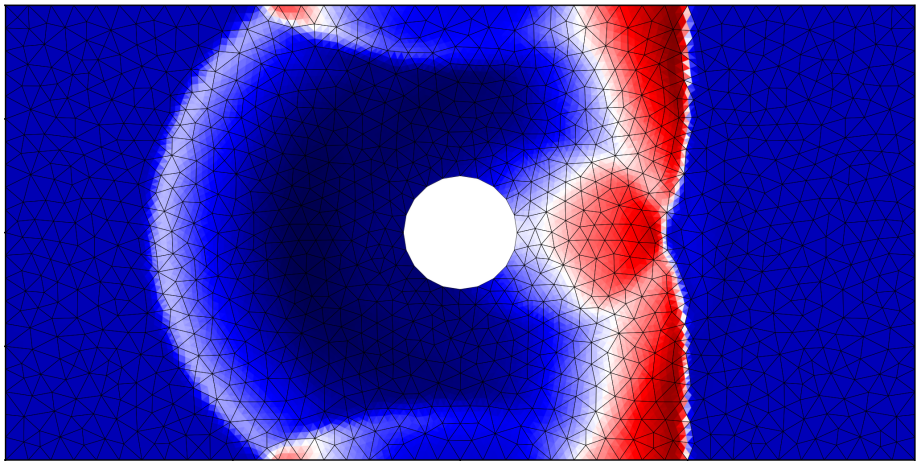

1. Wave hitting a fixed submerged cylinder obstacle (MP4),
2. Wave hitting a submerged moving pontoon object (MP4),
3. Wave generation by a prescribed motion of the floating structure (MP4).

↪ More simulations on my webpage!

Some qualitative simulations

But the object was supposed to be fixed?

Indeed, but in the **pseudo-1D pontoon configuration**, the model/numerics can actually be extended to:

- **Prescribed motion:** impose a given vertical trajectory to the object (this is the case in the wave-maker simulation),
- **Free motion:** couple the fluid system with an additional ODE expressing Newton's law for the vertical dynamics of the structure.

But I think that is enough equations for today ☺

1. Wave hitting a fixed submerged cylinder obstacle (MP4),
2. Wave hitting a submerged moving pontoon object (MP4),
3. Wave generation by a prescribed motion of the floating structure (MP4).

↪ More simulations on my webpage!

Table of contents

Slides available online at sachacardonna.github.io

Ongoing and upcoming work

What has been done...

S.C., A. Haidar, F. Marche & F. Vilar, *Local subcell monolithic DG/FV methods for nonlinear SW models with source terms*. Submitted. 2025.

S.C., F. Marche & F. Vilar, *An high-order scheme for 2D NSW equations with topography and friction effects on unstructured grids*. Submitted. 2026.

S.C., D. Lannes, F. Marche & F. Vilar, *Numerical resolution of 2D NSW equations with a partly immersed surface obstacle*. In preparation. 2026.

... and what are the plans for the future!

- Extension to **dispersive water-waves equations** (e.g. Green–Naghdi, Boussinesq) to capture more complex wave phenomena,
- Designing a model taking into account the **free motion** of the structure,
- Adaptation of the method to **moving** or **deforming** meshes via an **ALE framework**...

Currently: ALE framework for moving meshes (1)

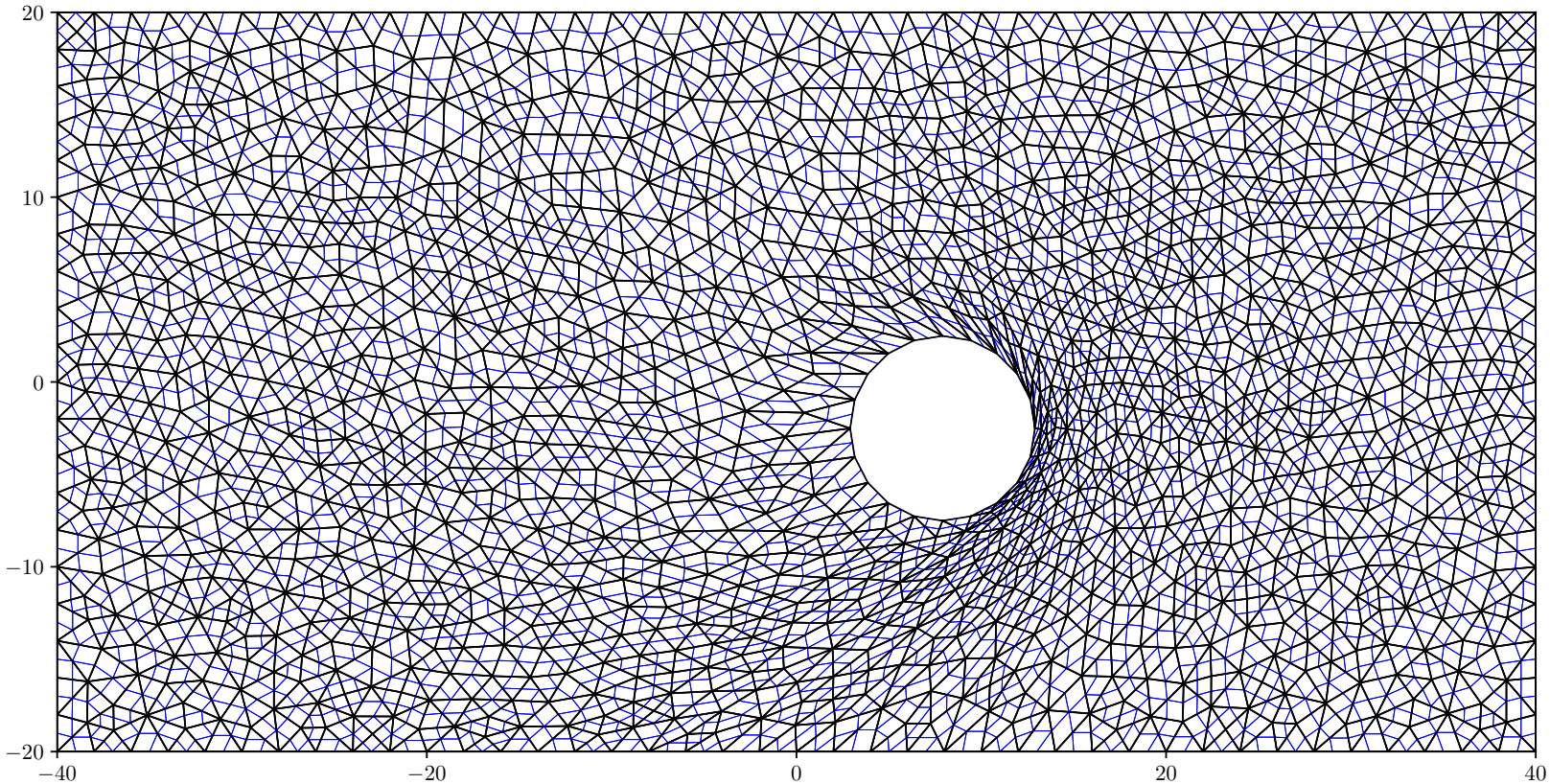

Figure: Comparison of nodal grid-velocity solvers: Laplacian smoothing (GIF).

$$
\begin{aligned}
-\nabla_{\boldsymbol{x}} \cdot \left(\kappa(\boldsymbol{x}) \nabla_{\boldsymbol{x}} \boldsymbol{w}^g\right) &= 0 \qquad && \text{in } \Omega(t), \\
\boldsymbol{w}^g &= \boldsymbol{0} \qquad && \text{on } \partial\Omega_{\text{ext}}, \\
\boldsymbol{w}^g &= \partial_t \boldsymbol{x}_{\text{mov}}(t) \qquad && \text{on } \partial\Omega_{\text{mov}}(t).
\end{aligned}
$$

Currently: ALE framework for moving meshes (2)

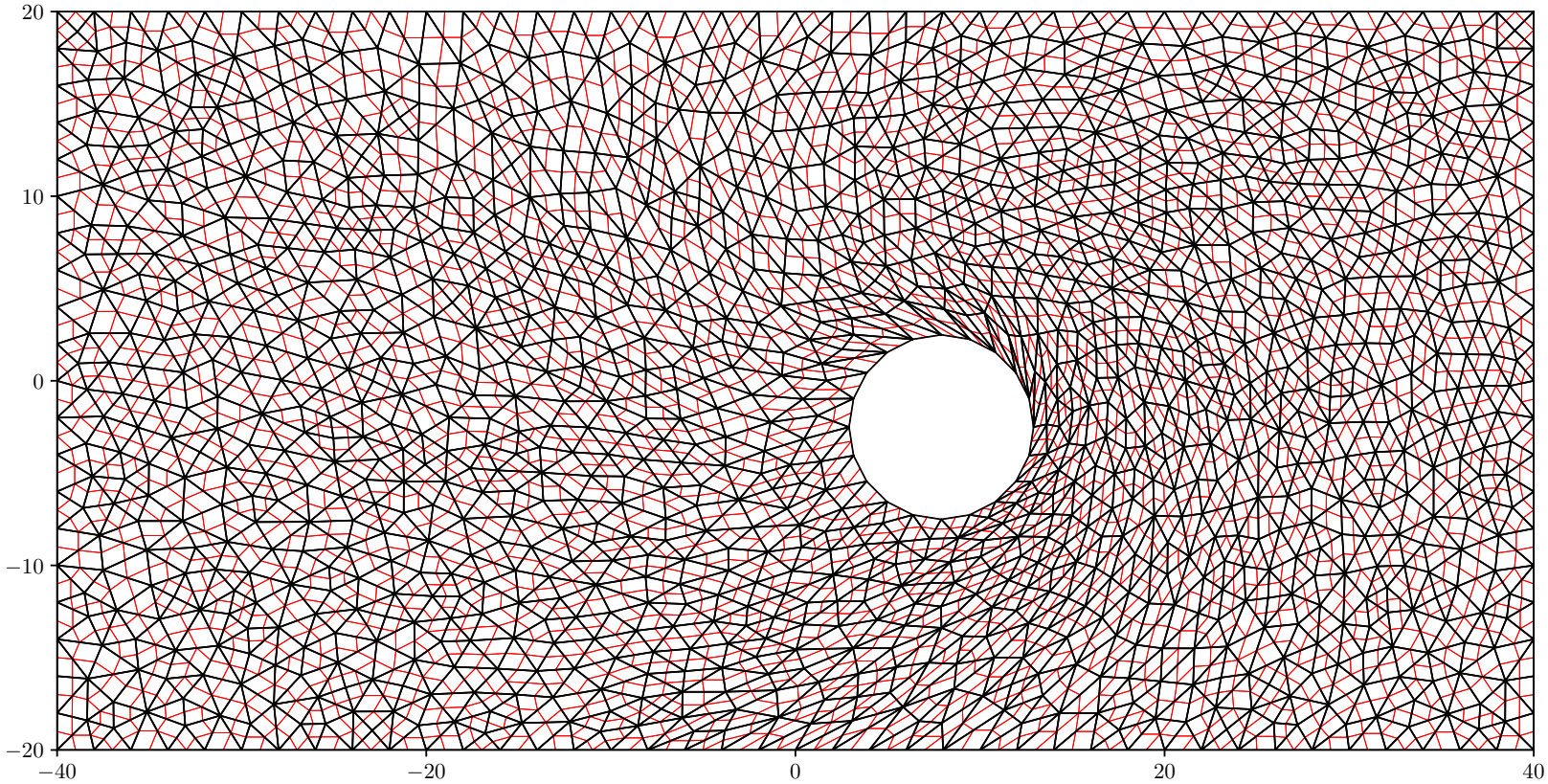

Figure: Comparison of nodal grid-velocity solvers: linear elasticity smoothing (GIF).

$$
\begin{aligned}
-\nabla_{\boldsymbol{x}} \cdot (2\mu(\boldsymbol{x})\boldsymbol{\varepsilon}(\boldsymbol{w}^g) + \lambda(\boldsymbol{x})(\nabla_{\boldsymbol{x}} \cdot \boldsymbol{w}^g)\mathbb{I}_2) &= \mathbf{0} && \text{in } \Omega(t),\\
\boldsymbol{\varepsilon}(\boldsymbol{w}^g) &:= \tfrac{1}{2}\left(\nabla_{\boldsymbol{x}}\boldsymbol{w}^g + (\nabla_{\boldsymbol{x}}\boldsymbol{w}^g)^\top\right) && \text{in } \Omega(t),\\
\boldsymbol{w}^g = \mathbf{0} \quad \text{on } \partial\Omega_{\text{ext}} \quad \text{and} \quad \boldsymbol{w}^g &= \partial_t \boldsymbol{x}_{\text{mov}}(t) && \text{on } \partial\Omega_{\text{mov}}(t).
\end{aligned}
$$

Currently: ALE framework for moving meshes (3)

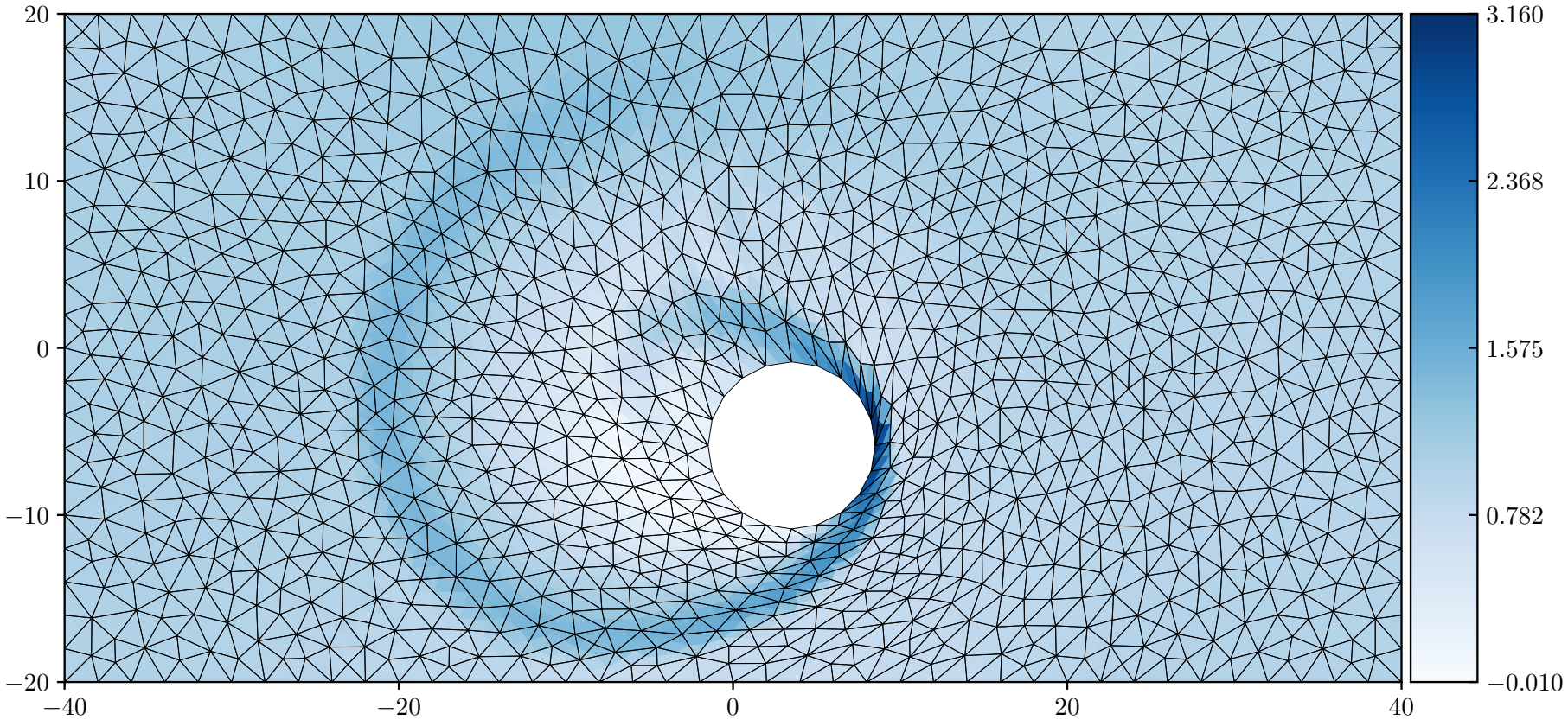

Figure: Local monolithic DG/FV–ALE method for NSW flows: preliminary results (MP4).

∼ Thank you for your attention! ∼

Special acknowledgments

- **Scientific committee of SHARK-FV26**

  ↪ *W. Boscheri, S. Clain, A. Del Grosso, M. Dumbser, G. Gassner, C. Fiorini, M. Han-Veiga, R. Loubère, X. Nogueira, G. Puppo, & P. Tsoutsanis*

- **My mentors and advisors**

  ↪ *F. Marche & F. Vilar*

- **Supportive professors**

  ↪ *A. Duran, D. Lannes, B. Mohammadi, P. Azerad, D. Le Roux, V. Perrier & D. Del Rey Fernández*

- **Colleagues and friends**

  ↪ *A. Haidar & M. Hanot*

Contact: *sacha.cardonna@umontpellier.fr*
Website: *sachacardonna.github.io*

Mesh subdivision

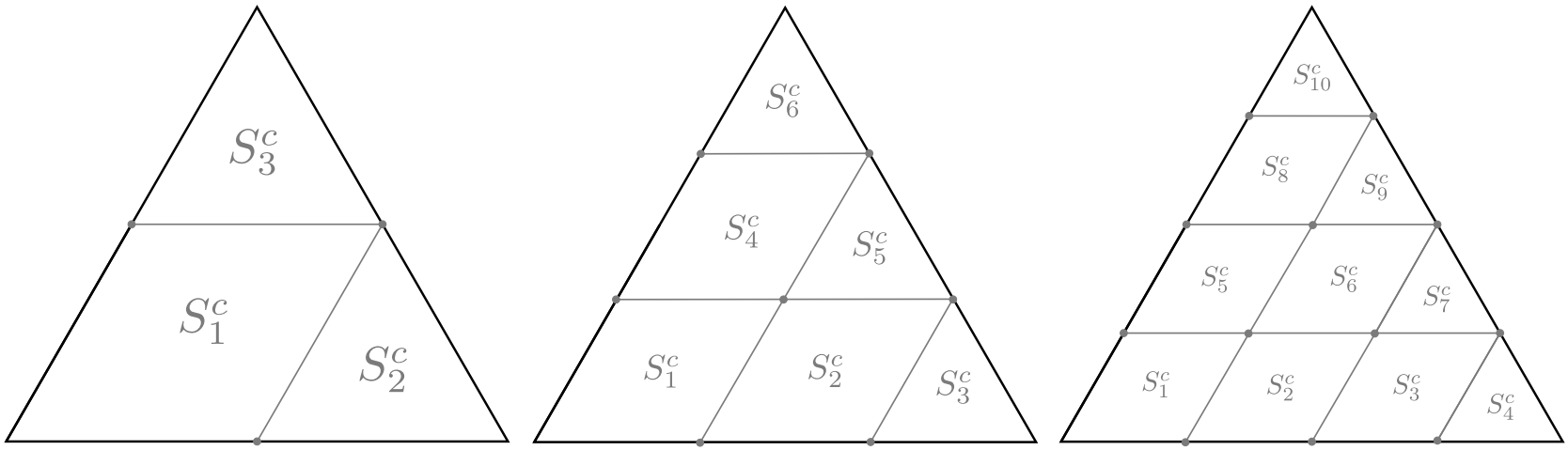

Cell ω_c subdivided into $N_s = N_k$ subcells for $\mathbb{P}^1$ (left), $\mathbb{P}^2$ (center) and $\mathbb{P}^3$ (right) cases

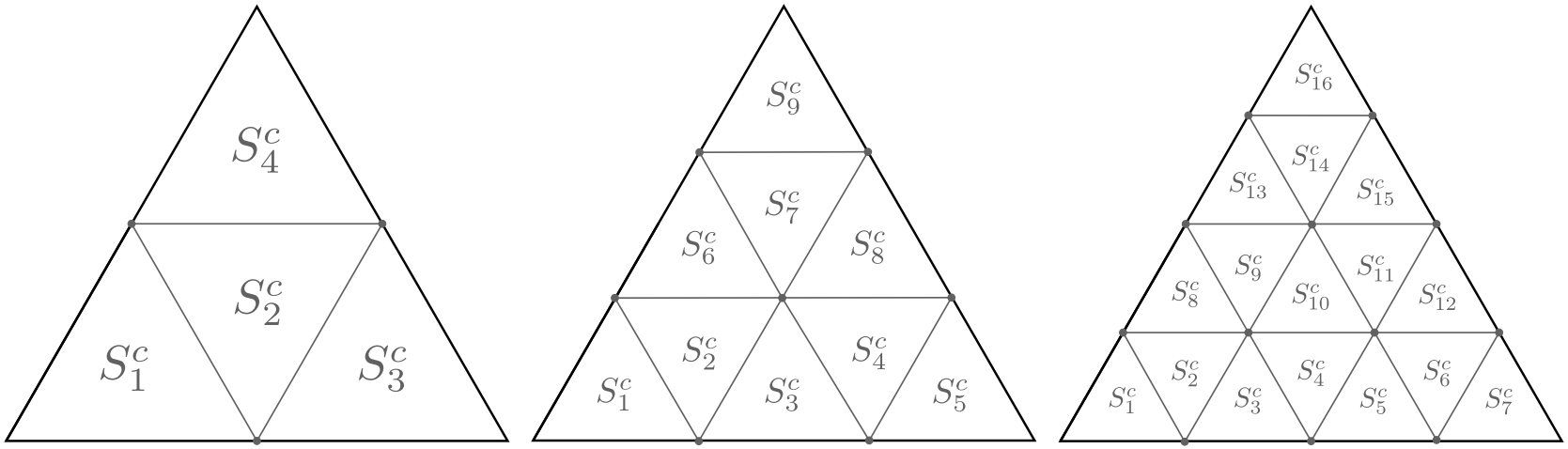

Cell ω_c subdivided into $N_s \geq N_k$ subcells for $\mathbb{P}^1$ (left), $\mathbb{P}^2$ (center) and $\mathbb{P}^3$ (right) cases

Subneighbors

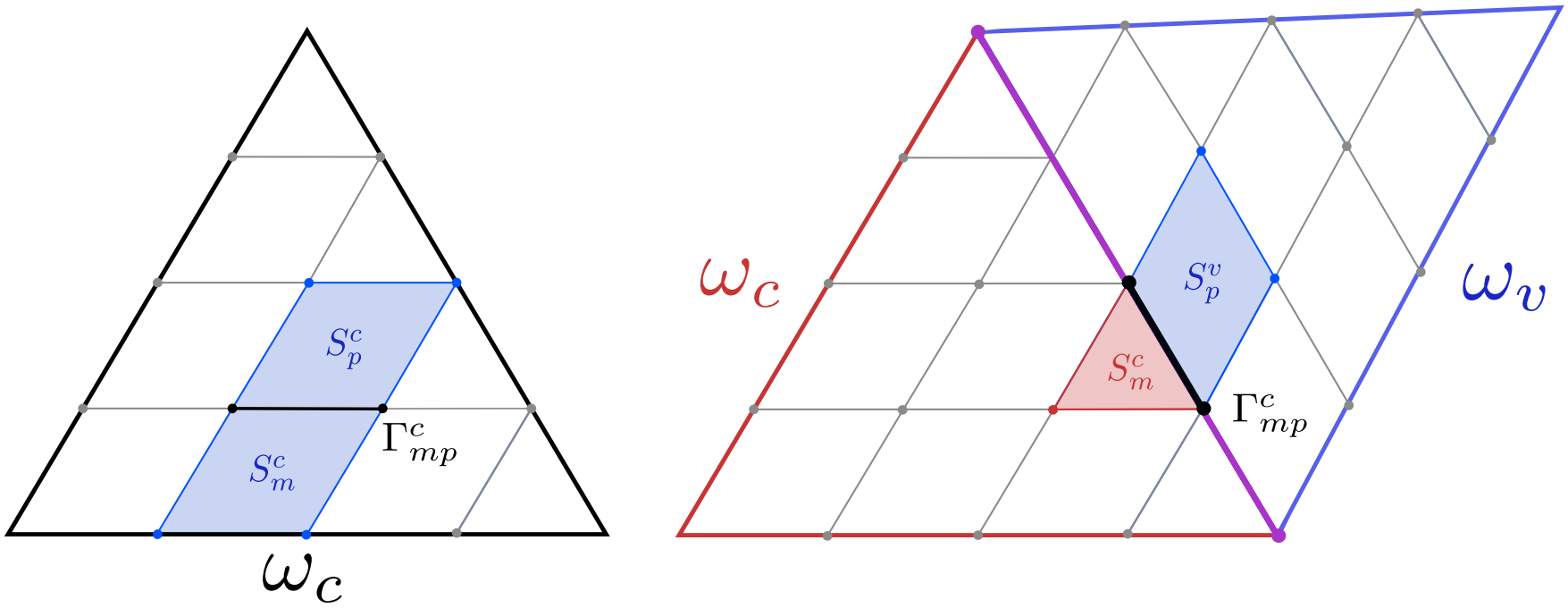

Figure: Two cases: subneighbor S_p inside cell ω_c (left), and subneighbor S_p inside neighbor cell ω_v (right).

Reconstructed DG fluxes (1)

Submean values vector derivative

Since $\mathbb{M}_c \dfrac{\mathrm{d}\boldsymbol{V}_c}{\mathrm{d}t} = \Phi_c + \boldsymbol{S}_c$ and $\overline{\boldsymbol{V}}_c = \mathbb{P}_c \boldsymbol{V}_c \implies$ $\boxed{\dfrac{\mathrm{d}\overline{\boldsymbol{V}}_c}{\mathrm{d}t} = \mathbb{P}_c \mathbb{M}_c^{-1}(\Phi_c + \boldsymbol{S}_c)}$

Flux reconstruction to get a FV-like scheme

Let us consider the DG reconstructed flux $\widehat{\mathbb{F}}_n$ such that

$$\frac{\mathrm{d}\overline{\boldsymbol{v}}_m^c}{\mathrm{d}t} = -\frac{1}{|S_m^c|}\int_{\partial S_m^c} \widehat{\mathbb{F}}_n(\boldsymbol{x})\,\mathrm{d}\boldsymbol{x} + (\mathbb{P}_c\mathbb{M}_c^{-1}\boldsymbol{S}_c)_m \qquad \text{(FV-like scheme)}$$

$$= -\frac{1}{|S_m^c|}\sum_{S_p^v \in \mathcal{V}_m^c}\int_{\Gamma_{mp}^c} \widehat{\mathbb{F}}_n(\boldsymbol{x})\,\mathrm{d}\boldsymbol{x} + (\mathbb{P}_c\mathbb{M}_c^{-1}\boldsymbol{S}_c)_m \quad \left(\partial S_m^c = \cup_{S_p^v \in \mathcal{V}_m^c}\Gamma_{mp}^c\right)$$

$$= -\frac{1}{|S_m^c|}\left(\sum_{S_p^v \in \breve{\mathcal{V}}_m^c}\int_{\Gamma_{mp}^c} \widehat{\mathbb{F}}_n(\boldsymbol{x})\,\mathrm{d}\boldsymbol{x} + \int_{\partial\omega_c \cap \partial S_m^c} \mathbb{F}_n^*\,\mathrm{d}\boldsymbol{x}\right) + (\mathbb{P}_c\mathbb{M}_c^{-1}\boldsymbol{S}_c)_m$$

under the hypothesis that $\widehat{\mathbb{F}}_{n|\partial\omega} = \mathbb{F}^*$ for all $\omega \in \mathcal{T}_h$.

Reconstructed DG fluxes (2)

Interface reconstructed flux

We define $\widehat{\mathbb{F}}_{mp}$ at interface Γ^c_{mp} as: $\displaystyle\int_{\Gamma^c_{mp}} \widehat{\mathbb{F}}_n(\boldsymbol{x})\,\mathrm{d}\boldsymbol{x} = \varepsilon^c_{mp}\widehat{\mathbb{F}}_{mp}$,

where subface orientation is carried through ε^c_{mp}, such that $\varepsilon^c_{pm} = -\varepsilon^c_{mp}$.

Reconstructed flux system

$$\boxed{-\mathbb{A}_c\widehat{\mathbb{F}}_c = \mathbb{D}_c\frac{\mathrm{d}\overline{\boldsymbol{V}}_c}{\mathrm{d}t} + \partial\mathbb{F}_c}$$

- $(\widehat{\mathbb{F}}_c)_{mp} = |\Gamma^c_{mp}|\widehat{\mathbb{F}}_{mp}$ — **interior subfaces fluxes**
- $(\mathbb{A}_c)_{mp} = \varepsilon^c_{mp}$ — **adjacency matrix**
- $(\mathbb{D}_c)_m = |S^c_m|$ — **subvolume matrix**
- $(\partial\mathbb{F}_c)_m = \displaystyle\int_{\partial\omega_c\cap\partial S^c_m} \mathbb{F}^*_n\,\mathrm{d}\boldsymbol{x}$ — **cell boundary contribution**

⚠ Since $\ker\mathbb{A}_c \neq \{\mathbf{0}\}$, we use a *Graph Laplacian technique*

Reconstructed DG fluxes (3)

Residual definition of reconstructed fluxes

$$\boxed{\widehat{\mathbb{F}}_c = -\mathbb{A}_c^\top \mathscr{L}_c^{-1} \left(\mathbb{D}_c \mathbb{P}_c \mathbb{M}_c^{-1} \Phi_c + \partial \mathbb{F}_c \right)}$$

where $\mathscr{L}_c^{-1}$ is the gen. inverse of $\mathbb{L}_c := \mathbb{A}_c \mathbb{A}_c^\top$ on the orthogonal of its kernel:

$$\mathscr{L}_c^{-1} = (\mathbb{L}_c + \lambda \Pi)^{-1} - \frac{1}{\lambda} \Pi, \qquad \Pi = \frac{1}{N_s} (1 \otimes 1) \in \mathscr{M}_{N_k}, \qquad \forall \lambda \neq 0$$

R. Abgrall, *Some Remarks about Conservation for Residual Distribution Schemes*. Methods Appl. Math., 18:327-351, 2018.

Few remarks

- **Source term** is excluded in the definition since only flux-dependent integrals are considered in reconstruction,
- **Implementation**: only Φ_c and boundary terms $\partial \mathbb{F}_c$ depend on time, but all the other terms are precomputable,
- **Alternative expression**: using spanning set of subresolution functions $\phi_m^c = p_{\omega_c}^k(\mathbb{1}_m^c)$, where $p_{\omega_c}^k$ is the L^2-projector on cell ω_c.

Source term treatment

Flowchart of the discretization

Dealing with both **polynomial DOFs** and **subcell-averaged values**

1. **Subcell averages**: compute the submean values of the quantities involved on each subcell, then reconstruct polynomials via projection matrix $\mathbb{P}_c$,
2. **Projection**: evaluate $\boldsymbol{B}(\boldsymbol{v}_h)$ at quadrature nodes, then apply an L^2 projection onto $\mathbb{P}^k$,
3. **Integration**: compute the mean value of the projected source over each subcell:

$$\overline{\boldsymbol{B}}_m^c := \frac{1}{|S_m^c|} \int_{S_m^c} \boldsymbol{B}_h \, \mathrm{d}\boldsymbol{x}$$

Implementation remark

Formally corresponds to multiplying the DG source integral by $\mathbb{P}_c \mathbb{M}_c^{-1}$:

$$\overline{\boldsymbol{B}}_m^c = \mathbb{P}_c \mathbb{M}_c^{-1} \left(\int_{\omega_c} \boldsymbol{B}_h \varphi_h \, \mathrm{d}\boldsymbol{x} \right)$$

Generalization to algebraic/geometric source terms

Topography and (nonlinear) friction effects

$$\boxed{\boldsymbol{S}[b](\boldsymbol{v}) := \boldsymbol{B}[b](\boldsymbol{v}) + \boldsymbol{R}[b](\boldsymbol{v})}$$

- $\boldsymbol{B}[b](\boldsymbol{v}) = (0, -g\eta\nabla_{\boldsymbol{x}} b)^\top$ **Topography source term**
- $\boldsymbol{R}[b](\boldsymbol{v}) = \begin{cases} \left(0, -k_f^2\, \boldsymbol{q}\right)^\top, \ k_f > 0 & \textbf{Linear friction law} \\ \left(0, -n_f^2\, \dfrac{\boldsymbol{q}\,\|\boldsymbol{q}\|}{(\eta - b)^\gamma}\right)^\top, \ n_f, \gamma > 0 & \textbf{Manning friction law} \end{cases}$

❓ Handled the same way as previously → **easily generalizable**

Applications to Serre–Green–Naghdi (SGN) dispersive equations

Reformulation: Elliptic problem + NSW with dispersive source term

1. Elliptic problem solved *independently*, using a finite element method;
2. Resulting dispersive source term discretized within the NSW framework.

Reformulation as a Godunov-like scheme

Solution at t^{n+1} as a convex combination of quantities defined at t^n

$$\overline{\boldsymbol{v}}_m^{c,n+1} = \overline{\boldsymbol{v}}_m^{c,n} - \frac{\Delta t^n}{|S_m^c|} \sum_{S_p^v \in \mathcal{V}_m^c} \ell_{mp} \widetilde{\mathbb{F}}_{mp} + \Delta t^n \overline{\boldsymbol{B}}_m^{c,n}$$

$$+ \frac{\Delta t^n}{|S_m^c|} \mathbb{F}\left(\overline{\boldsymbol{v}}_m^{c,n}\right) \cdot \sum_{S_p^v \in \mathcal{V}_m^c} \ell_{mp} \mathbf{n}_{mp} \pm \frac{\sigma \Delta t^n}{|S_m^c|} \sum_{S_p^v \in \mathcal{V}_m^c} \ell_{mp} \overline{\boldsymbol{v}}_m^{c,n}$$

$$= \left(1 - \frac{\sigma \Delta t^n}{|S_m^c|} \sum_{S_p^v \in \mathcal{V}_m^c} \ell_{mp}\right) \overline{\boldsymbol{v}}_m^{c,n} + \frac{\sigma \Delta t^n}{|S_m^c|} \sum_{S_p^v \in \mathcal{V}_m^c} \ell_{mp} \widetilde{\boldsymbol{v}}_{mp}^{*,-} + \Delta t^n \overline{\boldsymbol{B}}_m^{c,n}$$

- $\widetilde{\boldsymbol{v}}_{mp}^*$ are the **blended Riemann intermediate states**

$$\widetilde{\boldsymbol{v}}_{mp}^* := \overline{\boldsymbol{v}}_m^{c,n} - \frac{\widetilde{\mathbb{F}}_{mp} - \mathbb{F}\left(\overline{\boldsymbol{v}}_m^{c,n}\right) \cdot \mathbf{n}_{mp}}{\sigma} = \boldsymbol{v}_{mp}^* - \Theta_{mp} \left(\frac{\widehat{\mathbb{F}}_{mp} - \mathbb{F}_{mp}^{*,\mathrm{FV}}}{\sigma} \right),$$

- $\boldsymbol{v}_{mp}^*$ are the 1^{st}**-order FV Riemann intermediate states**.

Analytical formula to ensure water height positivity

Relying on 1^{st}-order FV Riemann intermediate states

Proof of the natural **preservation of water-height positivity** for 1^{st}-order elevation Riemann FV states $\eta_{mp}^{*,\pm}$

$\hookrightarrow$ allows us to rely on the **robustness of FV framework** to ensure the properties we want

Physical admissibility detector

$$\boxed{\Theta_{mp}^{\mathscr{H}_b^+} := \min\left(\Theta_{mp}^{\mathscr{H}_b^+,-}, \Theta_{mp}^{\mathscr{H}_b^+,+}\right)}$$

- $\Theta_{mp}^{\mathscr{H}_b^+,-} := \dfrac{\sigma\left(\eta_{mp}^* - \overline{b}_m^c\right)}{\Delta\mathbb{F}_{mp}}$ if $\Delta\mathbb{F}_{mp} > 0$, $\Theta_{mp}^{\mathscr{H}_b^+,-} = 1$ else;
- $\Theta_{mp}^{\mathscr{H}_b^+,+} := \dfrac{\sigma\left(\overline{b}_p^v - \eta_{mp}^*\right)}{\Delta\mathbb{F}_{pm}}$ if $\Delta\mathbb{F}_{pm} < 0$, $\Theta_{mp}^{\mathscr{H}_b^+,+} = 1$ else.

Analytical formula to prevent spurious oscillations

Mimicking a local maximum principle

$$\alpha_m^c := \min_{S_p^v \in \mathcal{N}(S_m^c)} \overline{\eta}_p^{v,n} \leq \overline{\eta}_m^{c,n+1} \leq \max_{S_p^v \in \mathcal{N}(S_m^c)} \overline{\eta}_p^{v,n} =: \beta_m^c$$

where $\mathscr{P}_m^c$ is the set of vertices $\boldsymbol{x}_p$ of subcell S_m^c and

$$\mathcal{N}(S_m^c) := \bigcup_{\boldsymbol{x}_p \in \mathscr{P}_m^c} \{S_q \mid \boldsymbol{x}_p \in S_q\}$$

Subcell numerical admissibility detector

$$\Theta_{mp}^{\text{SubNAD}} := \min\left(1, \left|\frac{\sigma}{\Delta\mathbb{F}_{mp}}\right| \begin{cases} \min\left(\beta_p^v - \eta_{mp}^{*,+},\ \eta_{mp}^{*,-} - \alpha_m^c\right) & \text{if } \Delta\mathbb{F}_{mp} > 0 \\ \min\left(\beta_m^c - \eta_{mp}^{*,-},\ \eta_{mp}^{*,+} - \alpha_p^v\right) & \text{if } \Delta\mathbb{F}_{mp} < 0 \end{cases}\right)$$

⚠ For NSW, no local maximum principle for the conserved variable!

↪ needs to be **relaxed** in the presence of **smooth extremas**

Preservation of steady-states (1)

Why does it matter ?

- **Preserves lake at rest steady states exactly**, avoiding spurious motions;
- **Reduces numerical errors** near equilibrium, especially when small perturbations are present;
- **Essential for wet/dry interfaces**, where small oscillations can destabilize the scheme.

Well-balancing (WB) property

Providing that the integrals of discrete formulation are exactly computed, we have the following result:

$$\forall n \in \mathbb{N}, \quad \forall \eta^e > 0, \quad (\eta_h^n = \eta^e \text{ and } \boldsymbol{q}_h^n = \mathbf{0}) \Longrightarrow \left(\eta_h^{n+1} = \eta^e \text{ and } \boldsymbol{q}_h^{n+1} = \mathbf{0}\right)$$

Preservation of steady-states (2)

Sketch of proof

Objective: showing that numerical fluxes are cancelling the source term $i.e.$

$$\frac{1}{|S_m^c|}\sum_{S_p^v \in \mathcal{V}_m^c} \ell_{mp}\widetilde{\mathbb{F}}_{mp} = \overline{\boldsymbol{B}}_m^{c,n} \qquad \text{s.t.} \qquad \overline{\boldsymbol{v}}_m^{c,n+1} = \overline{\boldsymbol{v}}_m^{c,n}.$$

- Exact integration required → natural with high-order quadrature;
- Under well-balanced assumptions:
$$\nabla_{\boldsymbol{x}} \cdot \mathbb{F}(\boldsymbol{v}_c, b_c) = \boldsymbol{B}(\boldsymbol{v}_c, \nabla_{\boldsymbol{x}} b_c), \quad \forall \omega_c \subset \Omega_{\mathrm{f}},$$
- Fluxes $\widehat{\mathbb{F}}_{mp}$ and $\mathbb{F}_{mp}^{*,\mathsf{FV}}$ match the continuous flux $\mathbb{F}_h^c \cdot \mathbf{n}_{mp}$ under equilibrium;
- $\widetilde{\mathbb{F}}_{mp}$ is built as a convex combination of these well-balanced fluxes $\hookrightarrow$ preserves equilibrium as well !

Test 1 – Order of accuracy assessment

Steady vortex with $\mathscr{C}^\infty$ topography

- **Domain:** $\Omega = [-5,5]^2$ **Degree:** $k = 1,2,3$ **Mesh:** $n_{\text{el}} = 200 \rightarrow 12800$
- **Goal:** convergence of the scheme on a smooth solution with a consistent discretization of the topography source term

k	1		2		3	
h	$E^\eta_{L^2}$	$q^\eta_{L^2}$	$E^\eta_{L^2}$	$q^\eta_{L^2}$	$E^\eta_{L^2}$	$q^\eta_{L^2}$
1	9.445E-2	2.35	1.529E-2	2.91	4.580E-3	4.19
$\frac{1}{2}$	1.854E-2	2.16	2.039E-3	3.03	2.505E-4	4.10
$\frac{1}{4}$	4.158E-3	2.07	2.491E-4	2.97	1.465E-5	4.00
$\frac{1}{8}$	9.923E-4	–	3.187E-5	–	9.165E-7	–

Figure: L^2-errors between numerical and analytical solutions and convergence rates for η at time $t = 0.1$ sec.

Test 2 – Riemann problem

Dam-break on a wet bed

- **Domain:** $\Omega = [0, 1000] \times [0, 200]$ **Degree:** $k = 4$ **Mesh:** $n_{\text{el}} = 350$
- **Goal:** handling shock waves and rarefaction fronts

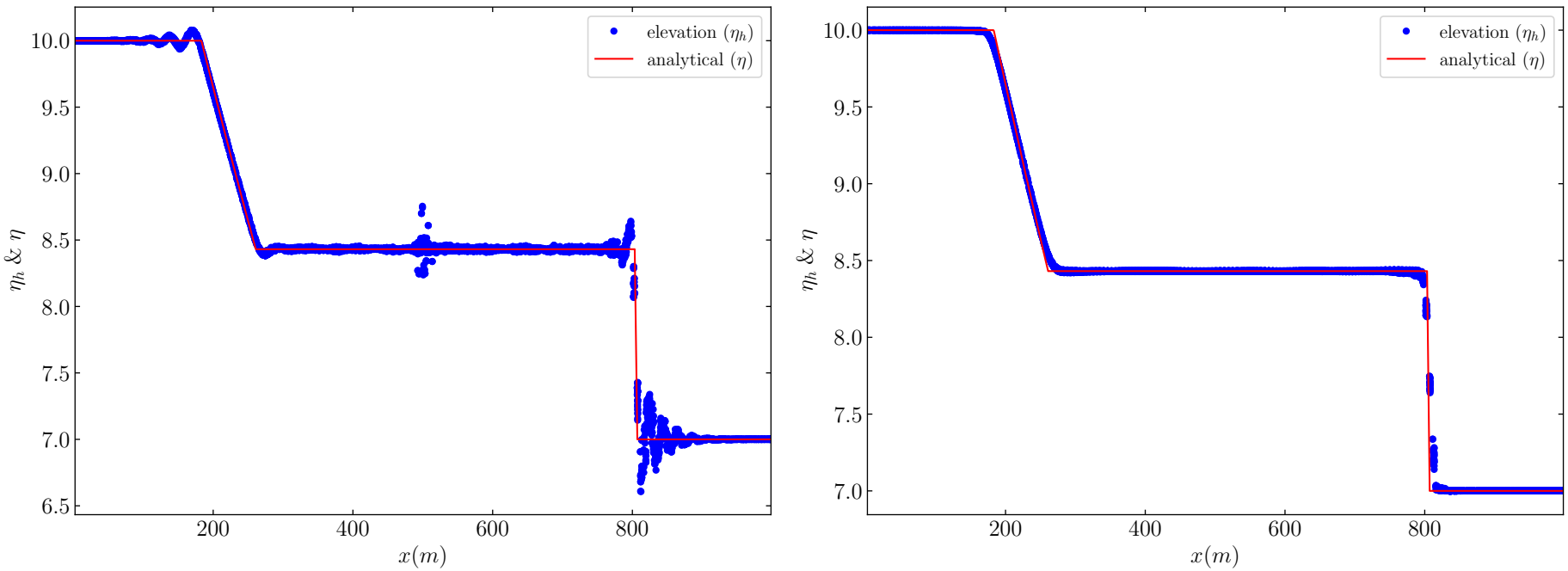

Figure: At $t = 32$ sec, $\mathbb{P}^4$ pure DG elevation (left) and monolithic DG/FV subcells elevation (right).

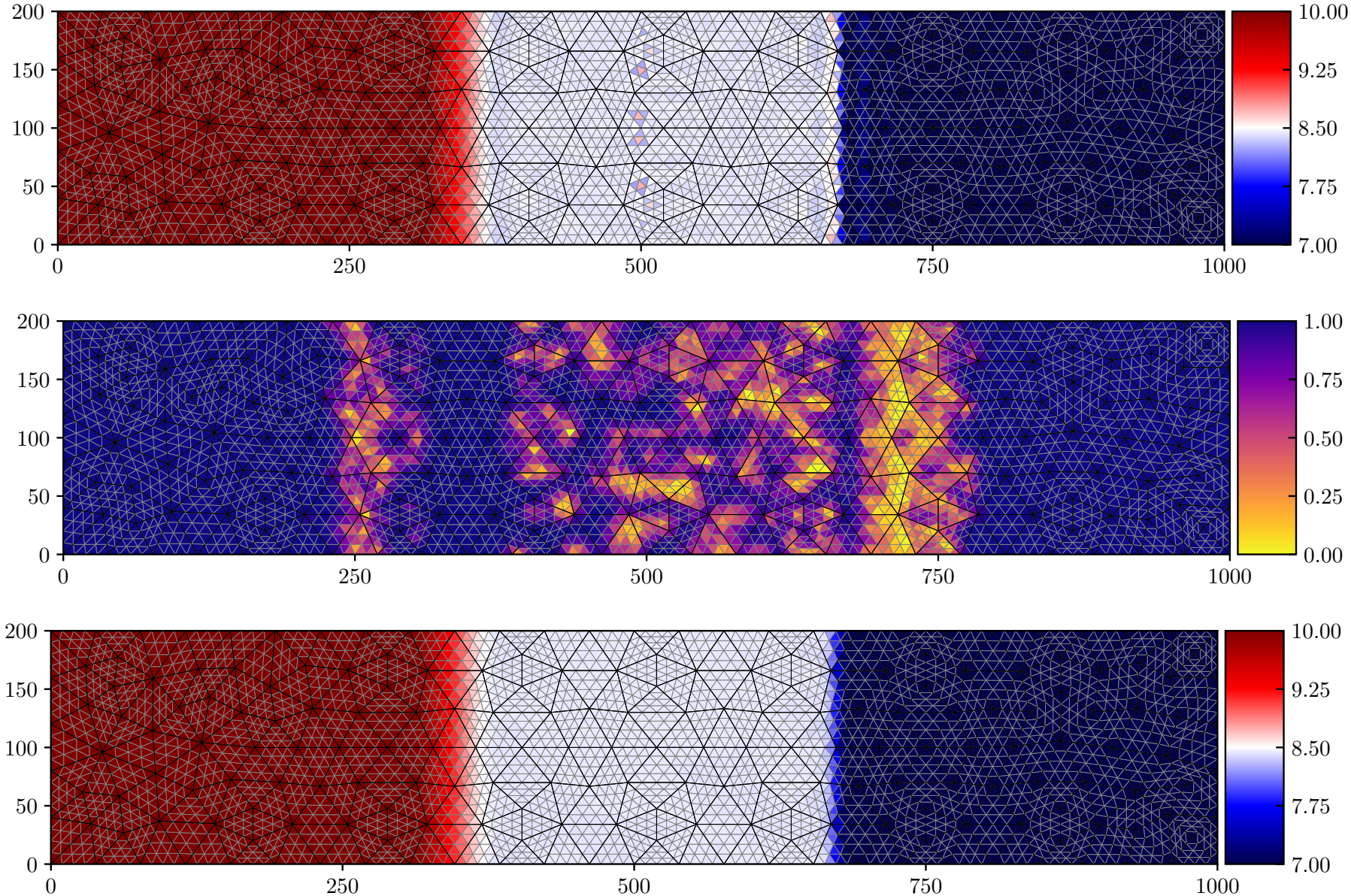

Figure: At $t = 18$ sec, $\mathbb{P}^4$ unlimited DG elevation (top), map of blending coefficient means per subcell (center) and monolithic DG/FV subcells elevation (bottom).

Test 3 – Periodic run-up/run-down

Carrier & Greenspan periodic solution

- **Domain:** $\Omega = [-20, 6] \times [0, 4]$ **Degree:** $k = 2$ **Mesh:** $n_{\text{el}} = 1092$
- **Goal:** assessing the ability of the scheme to capture periodic solutions on a dry bed with no phase shift

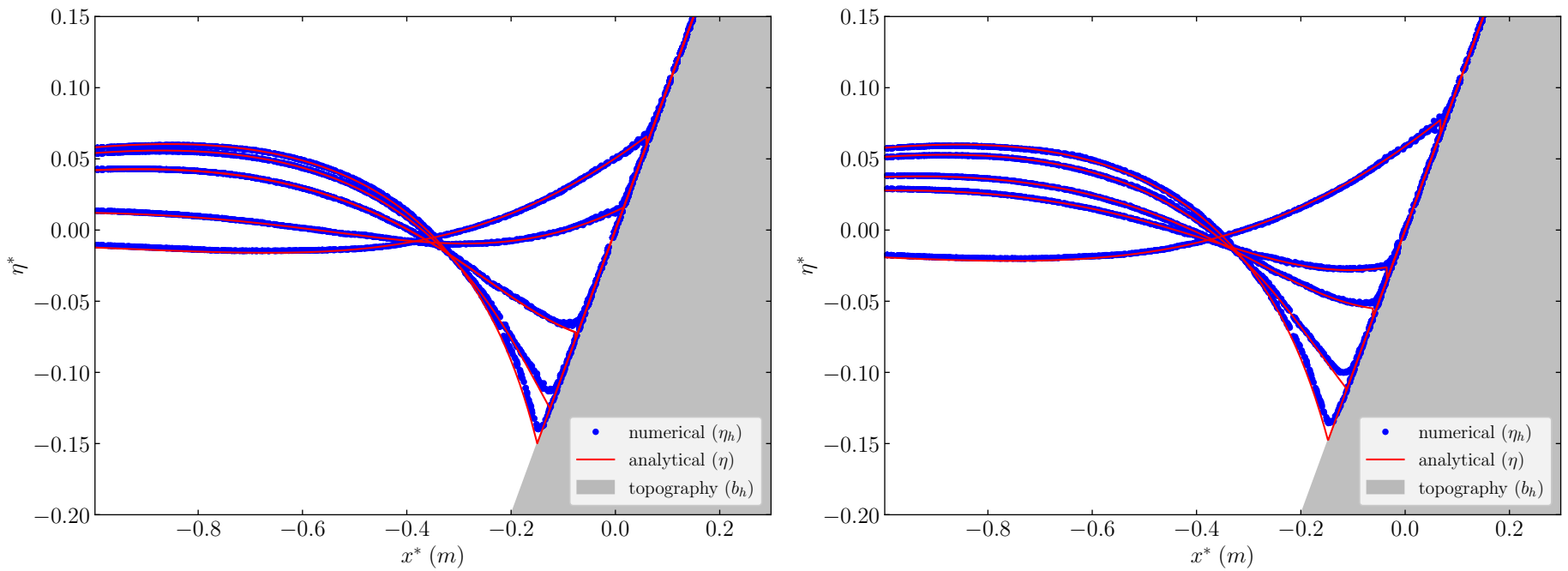

Figure: Snapshots of $\mathbb{P}^2$ elevation for $t \in [80, 86]$ sec (left) and for $t \in [154, 160]$ sec (right).

Test 4 – Rock-wave interactions

Single wave collapsing on a Gaussian rock

- **Domain:** $\Omega = [5, 25] \times [0, 30]$ **Degree:** $k = 6$ **Mesh:** $n_{\text{el}} = 584$
- **Goal:** assessing robustness and correct shock-capturing in challenging case

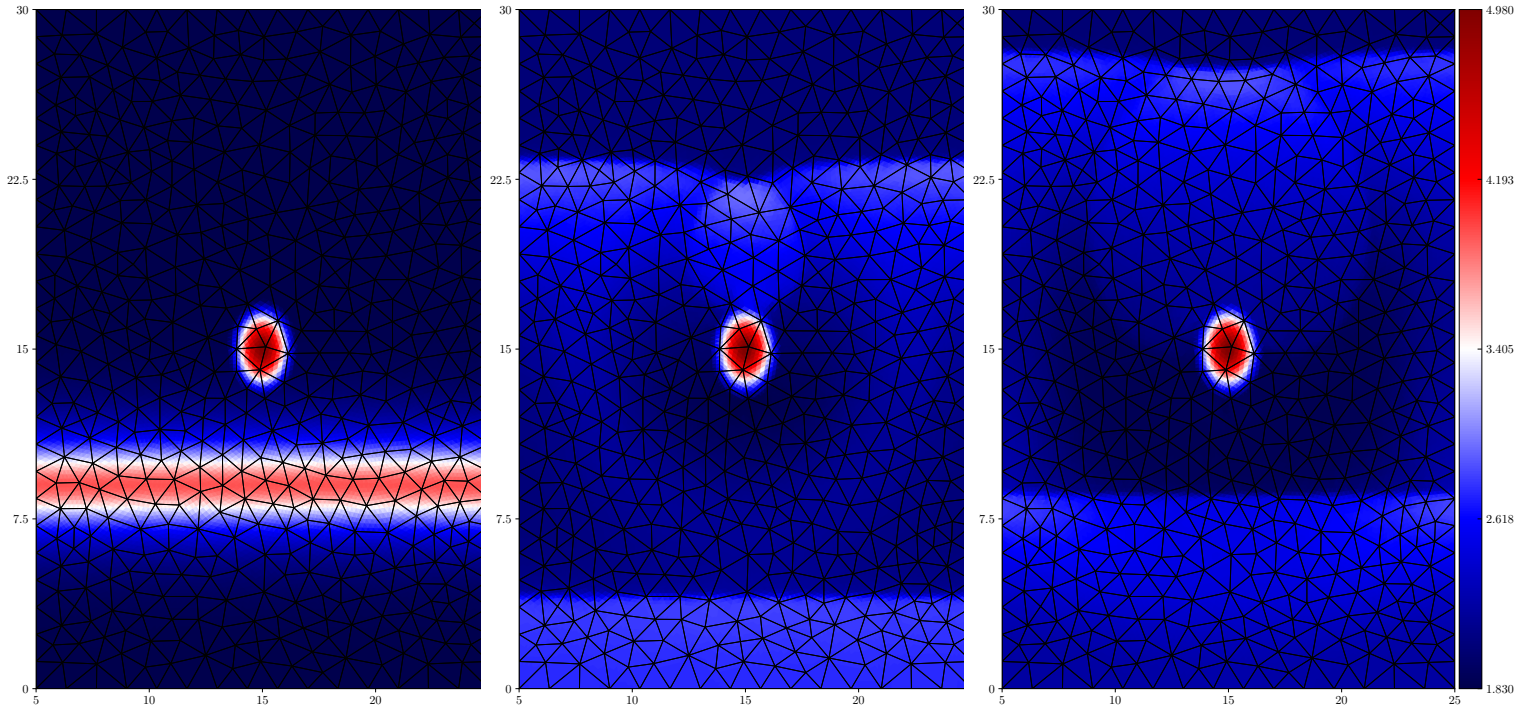

Figure: Snapshots of $\mathbb{P}^6$ elevation at several times (and link to simulation).